Published in "The Journal of Comparative Neurology 512(1):
27 - 51, 2009" which should be cited to refer to this work.

Postmortem Changes in the Neuroanatomical Characteristics of the Primate Brain: Hippocampal Formation

PIERRE LAVENEX,[1]* PAMELA BANTA LAVENEX,[1] JEFFREY L. BENNETT,[2] AND DAVID G. AMARAL[2]
[1]Department of Medicine, Unit of Physiology, University of Fribourg, 1700 Fribourg, Switzerland
[2]Department of Psychiatry and Behavioral Sciences, Center for Neuroscience, California National Primate Research Center and the M.I.N.D. Institute, UC Davis, Sacramento, California 95817, USA

ABSTRACT

Comparative studies of the structural organization of the brain are fundamental to our understanding of human brain function. However, whereas brains of experimental animals are fixed by perfusion of a fixative through the vasculature, human or ape brains are fixed by immersion after varying postmortem intervals. Although differential treatments might affect the fundamental characteristics of the tissue, this question has not been evaluated empirically in primate brains. Monkey brains were either perfused or acquired after varying postmortem intervals before immersion-fixation in 4% paraformaldehyde. We found that the fixation method affected the neuroanatomical characteristics of the monkey hippocampal formation. Soma size was smaller in Nissl-stained, immersion-fixed tissue, although overall brain volume was larger as compared to perfusion-fixed tissue. Nonphosphorylated high-molecular-weight neurofilament immunoreactivity was lower in CA3 pyramidal neurons, dentate mossy cells, and the entorhinal cortex, whereas it was higher in the mossy fiber pathway in immersion-fixed tissue. Serotonin-immunoreactive fibers were well stained in perfused tissue but were undetectable in immersion-fixed tissue. Although regional immunoreactivity patterns for calcium-binding proteins were not affected, intracellular staining degraded with increasing postmortem intervals. Somatostatin-immunoreactive clusters of large axonal varicosities, previously reported only in humans, were observed in immersion-fixed monkey tissue. In addition, calretinin-immunoreactive multipolar neurons, previously observed only in rodents, were found in the rostral dentate gyrus in both perfused and immersion-fixed brains. In conclusion, comparative studies of the brain must evaluate the effects of fixation on the staining pattern of each marker in every structure of interest before drawing conclusions about species differences.

Indexing terms: hippocampus; primate; human; Nissl; immunohistochemistry; perfusion; immersion; species differences; rhesus monkey; *Macaca mulatta*

Comparative studies of the structural organization of the brain are fundamental to our understanding of human brain function. However, whereas the brains of experimental animals are typically perfused with a fixative solution through the vasculature of deeply anesthetized subjects, human or ape brains are generally fixed by immersion after varying postmortem intervals. Although it is well known that the use of different fixative solutions can impact the staining properties of tissue, especially for immunohistochemistry (Lavenex, 2008), the use of the same fixative solution to fix tissue by perfusion versus immersion has not been considered a significant source of confound for comparative studies. It is nevertheless reasonable to consider that different fixation procedures might differentially affect the fundamental characteristics of the tissue. To date, however, this hypothesis has not been tested empirically in primate brains.

The present study compares the morphological and neurochemical characteristics of the monkey hippocampal formation following either perfusion or immersion fixation in 4% paraformaldehyde (PFA). The primate hippocampal formation proves to be an ideal structure for this type of study for three significant reasons: 1) the hippocampal formation is conserved across mammalian species; 2) the hippocampal formation consists of a large number of different cell types that might be differentially affected by perfusion method; and 3)

Grant sponsor: National Institutes of Health (NIH); Grant number: R01-NS16980; Grant sponsor: Swiss National Science Foundation; Grant number: PP00A-106701; conducted, in part, at the California National Primate Research Center (RR00169).

*Correspondence to: Dr. Pierre Lavenex, Dept. of Medicine, Unit of Physiology, University of Fribourg, Chemin du Musée 5, 1700 Fribourg, Switzerland. E-mail: pierre.lavenex@unifr.ch

changes in the morphological and neurochemical characteristics of the different structures comprising the hippocampal formation have been reported in patients with a variety of disease states, making the results of this study particularly relevant for studies of human pathology.

A previously published review of the chemical neuroanatomy of the primate hippocampal formation compared the distribution of numerous neurochemical markers in the monkey and human hippocampal formation (Kobayashi and Amaral, 1999). It has never been clear, however, whether certain reported differences in the neurochemical characteristics of the monkey and human brains are true species differences, or related, rather, to the use of different fixation methods or the inevitable postmortem delay between death and fixation of human tissue. It is difficult or impossible to obtain human histological material that has undergone experimental manipulation of fixation and postmortem parameters in order to study the effects of these procedures on brain morphology. Thus, it is first necessary to analyze, in a controlled manner, the effects of the method of fixation and postmortem delay on morphological and immunohistochemical features in the hippocampal formation of an appropriate animal model brain, such as that of the macaque monkey, that can provide a proxy for the human brain.

For this study we selected eight neurochemical markers based on their widespread use in previous monkey and human studies. For each neurochemical marker or staining procedure, we first describe the overall staining pattern in perfusion-fixed tissue (referring the reader to previously published articles for more detailed accounts of the regional and cellular distribution of each specific marker). We also provide basic descriptions of the distribution of some neurochemical markers in defined hippocampal regions that have not been previously described in the rhesus macaque monkey (*Macaca mulatta*). We then describe in detail the distribution or labeling pattern of each marker with respect to the method of fixation or the postmortem interval. Finally, we discuss our findings in relation to potential species differences previously reported in the literature. In particular, some findings from the current study corroborate previous evidence for true species differences, whereas others refute some claims of species differences, suggesting that they are most likely due to methodological differences.

The majority of the observations reported in this study are based on the immunohistochemical visualization of different peptides in the macaque monkey hippocampal formation. It is therefore particularly important to consider the specificity of the antibodies used, as well as the necessary or appropriate controls to determine their specificity. An editorial in this journal by Saper and Sawchenko (2003), as well as a recent article by Holmseth et al. (2006), have articulated some of the limitations of immunohistochemical procedures and these methods' tendency to produce spurious results. In sum, because antibodies are biological agents, tests for specificity can never be considered to be absolute, but rather must be considered to represent a failure to detect crossreactivity. Moreover, antibody staining should always be considered to label "antigen-like" molecules rather than staining the actual antigen (Saper and Sawchenko, 2003).

We have designed the present experiment with these limitations in mind. For example, we chose neurochemical markers that have already been well described in monkeys and/or humans. We performed a number of verification procedures based on the suggestions by Saper and Sawchenko (2003) and Holmseth et al. (2006). Specifically, we evaluated the specificity of the immunohistochemical patterns by: 1) omitting the primary antibody to see if the procedure resulted in complete absence of labeling; and 2) using several primary antibodies directed toward different antigens with nonoverlapping distributions (Holmseth et al., 2006). We also discuss some of our findings that might possibly be the result of the antibodies binding to something other than the antigen of interest (Holmseth et al., 2006). However, although we recognize that antibody staining should always be considered to label "antigen-like" molecules rather than staining the actual antigen, we decided to use terms such as "parvalbumin-immunoreactivity" rather than "parvalbumin-like-immunoreactivity" in order to make this article more readable.

TABLE 1. Summary of Cases Used in the Study

Case	Fixation	Gender	Age (years)
PM-17-03	Perfusion	M	13
PM-15-03	Perfusion	F	4.5
PM-10-02	2 hours	M	17
PM-03-02	2 hours	F	9
PM-05-02	6 hours	M	13
PM-13-03	6 hours	F	7
PM-14-03	12 hours	M	7
PM-12-03	12 hours	F	17
PM-11-03	24 hours	M	12
PM-01-02	24 hours	F	14
PM-04-02	48 hours	M	8
PM-02-02	48 hours	F	10

MATERIALS AND METHODS

We prepared histological sections from rhesus monkey (*Macaca mulatta*) brains either perfused with 4% PFA following our laboratory's standard protocol (Lavenex et al., 2002, 2004a,b; Banta Lavenex et al., 2006) or fixed by immersion fixation in the same fixative (4% PFA) after postmortem intervals of 2, 6, 12, 24, or 48 hours. All protocols were approved by the Institutional Animal Care and Use Committee of the University of California, Davis, and were in accordance with the National Institutes of Health guidelines for the use of animals in research. Only neurologically unremarkable monkeys predestined to be culled for colony management were used in this study.

Brain collection

Perfused tissue. Two adult rhesus macaques (Table 1; one 13-year-old male and one 4.5-year-old female) were deeply anesthetized with intravenous injection of sodium pentobarbital (50 mg/kg i.v., Fatal-Plus, Vortech Pharmaceuticals, Dearborn, MI) and perfused transcardially with ice-cold 1% PFA in 0.1 M phosphate buffer (PB, pH 7.4) for 2 minutes at a rate of 250 mL/min, followed by ice-cold 4% PFA in 0.1 M PB (pH 7.4) for 10 minutes at a rate of 250 mL/min, then continued for another 50 minutes at a rate of 100 mL/min. The monkey's head was packed in ice for the entire duration of the perfusion. The brains were extracted immediately following perfusion and postfixed for 6 hours in the same fixative at 4°C under constant, gentle agitation. Brains were then immersed in a

cryoprotective solution made of 10% glycerol and 2% dimethyl sulfoxide (DMSO; Fisher Scientific, Waltham, MA) in 0.1 M PB for 24 hours at 4°C, followed by 72 hours in 20% glycerol and 2% DMSO in 0.1 M PB at 4°C. Finally, the brains were cut into three blocks in the coronal plane using a histological blade, then flash-frozen in isopentane (2-methylbutane, Fisher Scientific) cooled in a 100% ethanol dry-ice bath. The blocks were then wrapped with aluminum foil and stored at –70°C until cutting.

Immersion-fixed tissue. Ten adult rhesus macaques (one male and one female per timepoint, all between 7 and 17 years of age; Table 1) were euthanized with a lethal dose of sodium pentobarbital (100 mg/kg i.v.). Immediately after the time of death, i.e., cardiac arrest as determined by the senior veterinary pathologist at the California National Primate Research Center, monkeys' heads were cut off and placed at 4°C. After specific postmortem intervals (either 2, 6, 12, 24, or 48 hours), the brains were extracted and placed in 4% PFA for immersion-fixation for 48 hours under constant agitation. After fixation, brains were blocked, cryoprotected, and frozen as described previously for the perfused tissue.

Cutting and tissue storage

Brains were cut at a thickness of 30 μm on a freezing sliding microtome (Microm HM 440, Microm International, Germany). One-in-eight series of sections were collected in 10% formaldehyde solution in 0.1 M PB (pH 7.4) and postfixed at 4°C for 4 weeks prior to Nissl staining with thionin. All other series were collected in tissue collection solution (TCS) made of 25% glycerin, 20% dH_2O, 30% ethylene glycol, and 25% 0.2 M PB and kept at –70°C until further processing.

Nissl stain

The procedure for Nissl-stained sections was as follows: Sections were taken out of the 10% formaldehyde solution, thoroughly washed 2 × 2 hours in 0.1 M PB, mounted on gelatin-coated slides from filtered 0.05 M PB (pH 7.4), and air-dried overnight at 37°C. Sections were then defatted 2 × 2 hours in a mixture of chloroform/ethanol (1:1, vol.), and rinsed 2 × 2 minutes in 100% ethanol, 1 × 2 minutes in 95% ethanol, and air-dried overnight at 37°C. Sections were then rehydrated through a graded series of ethanol, 2 minutes in 95% ethanol, 2 minutes in 70% ethanol, 2 minutes in 50% ethanol, dipped in two separate baths of dH_2O, and stained 20 seconds in a 0.25% thionin (Fisher Scientific, Cat. no. T-409) solution, dipped in two separate baths of dH_2O, 4 minutes in 50% ethanol, 4 minutes in 70% ethanol, 4 minutes in 95% ethanol + glacial acetic acid (1 drop per 100 mL of ethanol), 4 minutes in 95% ethanol, 2 × 4 minutes in 100% ethanol, 3 × 4 minutes in xylene, and coverslipped with DPX (BDH Laboratories, Poole, UK).

Soma cell size was measured on Nissl-stained preparations, using the nucleator probe of StereoInvestigator 5.0 (MicroBrightField, Williston, VT). Briefly, the nucleator can be used to estimate the mean cross-sectional area and volume of cells. A set of rays emanating from a randomly chosen point within the nucleus or nucleolus is drawn and oriented randomly. The length of the intercept from the point to the cell boundary (l) is measured and the cell volume is obtained by $V = (4/3*3.1416)*l^3$. Essentially, this is the formula used to determine the volume of a sphere with a known radius. For each field, a total of 100 randomly chosen neurons in one section located at a mid-rostrocaudal level of the hippocampus were analyzed. A total of 10 perfusion-fixed brains (two brains from this study + eight brains prepared for other studies) and 10 immersion-fixed brains were used for this analysis.

Nonphosphorylated high-molecular-weight neurofilaments

The immunohistochemical procedure for visualizing nonphosphorylated high-molecular-weight neurofilaments was carried out on free-floating sections using the monoclonal antibody SMI-32 (Sternberger Monoclonals, Lutherville, MD, Cat. no. SMI-32, lot 16). This antibody was raised in mouse against the nonphosphorylated 200 kDa heavy neurofilament. On conventional immunoblots, SMI-32 visualizes two bands (200 and 180 kDa), which merge into a single NFH line on two-dimensional blots (Sternberger and Sternberger, 1983; Goldstein et al., 1987). This antibody has been shown to react with nonphosphorylated high-molecular-weight neurofilaments of most mammalian species, including rats, cats, dogs, monkeys, and humans (Siegel et al., 1993; Hof and Morrison, 1995; Hornung and Riederer, 1999; de Haas Ratzliff and Soltesz, 2000; Lavenex et al., 2004a), and may also show some limited crossreactivity with nonphosphorylated medium-molecular-weight neurofilaments (Hornung and Riederer, 1999).

Sections that had been maintained in TCS at –70°C were rinsed 3 × 10 minutes in 0.05 M Tris buffer (pH 7.4) with 1.5% NaCl, treated against endogenous peroxidase by immersion in 0.5% hydrogen peroxide solution in 0.05 M Tris/NaCl for 15 minutes and rinsed 6 × 5 minutes in Tris/NaCl buffer. Sections were then incubated for 4 hours in blocking solution made of 0.5% Triton X-100 (TX-100; Fisher Scientific, Cat. no. BP151-500), 10% normal horse serum (NHS; Biogenesis, Poole, UK; Cat. no. 8270-1004) in 0.05 M Tris/NaCl buffer at room temperature. Sections were then incubated overnight with the primary antibody SMI-32 (1:2,000) in 0.3% TX-100, 1% NHS in 0.05 M Tris/NaCl at 4°C. Sections were then washed 3 × 10 minutes in 0.05 M Tris/NaCl buffer with 1% NHS, incubated for 1 hour with a secondary antibody, biotinylated horse anti-mouse IgG (1:227; Vector Laboratories, Burlingame, CA; Cat. no. BA-2000) in 0.3% TX-100, 1% NHS in 0.05 M Tris/NaCl buffer, rinsed 3 × 10 minutes in 0.05 M Tris/NaCl buffer containing 1% NHS, incubated for 45 minutes in an avidin-biotin complex solution (Biostain ABC kit, Biomeda, Foster City, CA; Cat. no. 11-001), washed 3 × 10 minutes in Tris/NaCl, incubated in secondary antibody solution for another 45 minutes, washed 3 × 10 minutes, incubated in the avidin-biotin complex solution for 30 minutes, washed 1 × 10 minutes in 0.5 M Tris/NaCl and 2 × 10 minutes in 0.05 M Tris (no NaCl), incubated for 30 minutes in a solution containing 0.05% diaminobenzidine (DAB, Sigma-Aldrich Chemicals, St. Louis, MO; Cat. no. D9015-100MG), 0.04% H_2O_2 in 0.05 M Tris buffer, and washed 3 × 10 minutes. Sections were then mounted on gelatin-coated slides from filtered 0.05 M PB (pH 7.4) and air-dried overnight at 37°C. Reaction product was then intensified with a silver nitrate–gold chloride method (Lavenex et al., 2004b). Sections were defatted 2 × 2 hours in a chloroform/ethanol (1:1, vol.) solution, rehydrated through a graded series of ethanol, and air-dried overnight at 37°C. Sections were then rinsed 10 minutes in running dH_2O, incubated for 40 minutes in a 1% silver nitrate ($AgNO_3$) solution at 56°C, rinsed 10 minutes in dH_2O, incubated for 10 minutes in

0.2% gold chloride ($HAuCl_4$ $3H_2O$) at room temperature with agitation, rinsed 10 minutes in dH_2O, stabilized in 5% sodium thiosulfate ($Na_2S_2O_3$) for 15 minutes with agitation, rinsed in running dH_2O for 10 minutes, dehydrated through a graded series of ethanol and xylene, and coverslipped with DPX.

Acetylcholinesterase

Acetylcholinesterase distribution was visualized using two different methods: the enzymatic activity method, and the immunohistochemical method.

Enzymatic activity. The procedure for visualizing acetylcholinesterase enzymatic activity was carried out on free-floating sections using the Koelle acetylthiocholine method, as described previously (Bakst and Amaral, 1984). Staining patterns were comparable to those previously described in primates (see Results and Discussion sections for detailed description, comparison, and references). Sections that had been maintained in TCS at –70°C were rinsed 3 × 5 minutes in 0.1 M sodium acetate buffer (pH 6.0) and then incubated in a solution of anhydrous sodium acetate (65 mM), acetylthiocholine iodide (1.7 mM), sodium citrate (5 mM), copper sulfate (3 mM), potassium ferricyanide (0.2 mM), and ethopropazine (0.2 mM) in dH_2O. The incubation was carried out at room temperature for 30 minutes and, after the sections were washed thoroughly in 0.1 M sodium acetate solution (pH 6.0), they were placed in a solution of 4% ammonium sulphide and agitated gently for 1 minute and washed 3 × 5 minutes in 0.1 M sodium nitrate solution. The reaction product was then intensified by incubating the sections in a solution of 0.1% silver nitrate for 1 minute under constant agitation. Finally, the sections were washed 3 × 5 minutes in 0.1 M sodium nitrate and mounted, dehydrated in a graded series of ethanol, cleared in xylene, and coverslipped with DPX.

Immunohistochemistry. The second procedure for visualizing acetylcholinesterase distribution was carried out on free-floating sections using a monoclonal antibody anti-acetylcholinesterase (anti-AChE [HR2]; AbCam, Cambridge, MA; Cat. no. ab2803-200, lot 93493). This antibody was raised in mouse against purified human cerebellar acetylcholinesterase (68 kDa); it reacts with all mammalian AChEs tested, expect for those of mice and rats; this antibody does not react with butyrylcholinesterase in binding assays (Rakonczay and Brimijoin, 1988). Immunohistochemical staining pattern was consistent with that observed in tissue processed for the visualization of acetylcholinesterase enzymatic activity (see Results for detailed comparison). Sections that had been maintained in TCS at –70°C were rinsed 3 × 10 minutes in 0.02 M potassium PB (KPBS; pH 7.4), treated against endogenous peroxidase by immersion in 0.5% hydrogen peroxide solution in 0.02 M KPBS for 15 minutes, and rinsed 6 × 5 minutes in 0.02 M KPBS. Sections were then incubated for 4 hours in a blocking solution made of 0.5% TX-100, 10% horse serum (NHS, Biogenesis, Cat. no. 8270-1004) in 0.02 M KPBS at room temperature. Sections were then incubated overnight with the mouse anti-AChE monoclonal antibody (1:5,000) in 0.3% TX-100, 1% NHS in 0.02 M KPBS at 4°C. Sections were then washed 3 × 10 minutes in 0.02 M KPBS with 1% NHS, incubated for 1 hour with a secondary antibody, biotinylated horse antimouse IgG (1:227; Vector Laboratories, Cat. no. BA-2000) in 0.3% Triton X-100, 1% NHS in 0.02 M KPBS, rinsed 3 × 10 minutes in 0.02 M KPBS with 1% NHS, incubated for 45 minutes in an avidin-biotin complex solution (Biostain ABC kit, Biomeda, Cat. no. 11-001), washed 3 × 10 min in 0.02 M KPBS, incubated in secondary antibody solution for another 45 minutes, washed 3 × 10 minutes 0.02 M KPBS (no NHS), incubated in the avidin-biotin complex solution for 30 minutes, washed 3 × 10 minutes in 0.05 M Tris buffer, incubated for 30 minutes in a solution containing 0.05% diaminobenzidine (DAB, Sigma-Aldrich, Cat. no. D9015-100mg), 0.04% H_2O_2 in 0.05 M Tris buffer, and washed 3 × 10 minutes. Sections were then mounted on gelatin-coated slides from filtered 0.05 M PB (pH 7.4) and air-dried overnight at 37°C. Reaction product was then intensified with the silver nitrate-gold chloride method described above.

Serotonin

The procedure for visualizing serotonin-labeled fibers was carried out on free-floating sections using a rabbit anti-5-hydroxytryptamine (anti-5-HT) polyclonal antibody (Diasorin, Stillwater, MN; Cat. no. 20080, lot 909605; raised in rabbit against 5-HT conjugated to bovine serum albumin [BSA] with PFA). Specificity controls performed by the manufacturer indicate that: 1) this antiserum demonstrates significant labeling of rat hypothalamus, raphe nuclei, and spinal cord using biotin/avidin–horseradish peroxidase (HRP) techniques; staining is eliminated by pretreatment of the diluted antibody with serotonin/BSA. 2) Five μg, 10 μg, and 25 μg of either 5-hydroxytryptophan, 5-hydroxyindole-3-acetic acid, and dopamine do not react with the antiserum diluted at 1:20,000 using the biotin-streptavidin/HRP labeling method. Staining patterns were comparable to those previously described in primates (see Results and Discussion sections for detailed description, comparison, and references). Sections that had been maintained in TCS at –70°C were rinsed 3 × 10 minutes in 0.1 M phosphate-buffered saline (PBS; pH 7.4), treated against endogenous peroxidase by immersion in 0.5% hydrogen peroxide solution in 0.1 M PBS for 15 minutes, and rinsed 6 × 5 minutes in PBS solution. Sections were then incubated for 1 hour in a blocking solution of 0.4% TX-100, 5% normal goat serum (NGS; Biogenesis, Cat. no. 8270-1204), 2% BSA (fraction V, Sigma-Aldrich Chemicals; Cat. no. A-7638) in 0.1 M PBS at room temperature. Sections were then incubated overnight with the rabbit anti-5HT polyclonal antibody (1:10,000) in 0.1% TX-100, 1% NGS in 0.1 M PBS at 4°C. Sections were then washed 3 × 10 minutes in 0.1 M PBS, incubated for 1 hour at room temperature with a secondary antibody, goat antirabbit IgG (1:100; Vector Laboratories, Cat. no. AI-1000) in 0.1% TX-100, 1% NGS in 0.1 M PBS, rinsed 3 × 10 minutes in 0.1 M PBS solution containing 1% NGS. Sections were then incubated in rabbit peroxidase anti-peroxidase (PAP, 1:100; Sternberger Monoclonals, Lutherville, MD; Cat. no. 401) in 0.1 M PBS, 1% NGS and 0.1% TX-100 for 1 hour at room temperature with agitation. Sections were then rinsed 1 × 10 minutes in 0.1 M PBS and 2 × 10 minutes in 0.05 M Tris buffer (pH 7.4) before incubation for 2 minutes under constant agitation in a solution containing filtered 0.05% diaminobenzidine (DAB, Sigma-Aldrich, Cat. no. D9015–100mg), 0.015% H_2O_2 in 0.05 M Tris buffer. Finally, sections were washed 3 × 10 minutes, mounted on gelatin-coated slides from filtered 0.05 M PB, and air-dried overnight at 37°C. Reaction product was then intensified with the silver nitrate-gold chloride method described above.

Parvalbumin

The procedure for visualizing parvalbumin-positive fibers and cell bodies was carried out on free-floating sections using a mouse anti-parvalbumin monoclonal antibody (SWANT, Bellinzona, Switzerland; Cat. no. 235, lot 10-11F). This antibody is a mouse IgG produced by hybridization of mouse myeloma cells with spleen cells from mice immunized with parvalbumin purified from carp muscles. The antibody specifically stains the ^{45}calcium-binding spot of parvalbumin (MW 12,000, IEF 4.9) in a two-dimensional immunoblot. In radioimmunoassay it detects parvalbumin with a sensitivity of 10 ng/assay and an affinity of 7.9×10^{12} L/M (SWANT). Staining patterns were comparable to those previously described in primates (see Results and Discussion sections for detailed description, comparison, and references). Sections that had been maintained in TCS at –70°C were washed 3 × 10 minutes in 0.02 M KPBS (pH 7.4). To eliminate endogenous peroxidase activity, sections were treated with 1% H_2O_2 in dH_2O for 15 minutes, and then rinsed 6 × 5 minutes in 0.02 M KPBS. To block nonspecific binding, the sections were incubated in a solution containing 10% normal horse serum (NHS, Biogenesis, Cat. no. 8270-1004) and 0.5% TX-100 in 0.02 M KPBS for 4 hours at room temperature. Sections were then incubated with the mouse antiparvalbumin monoclonal antibody (1:5,000) in 0.5% TX-100 and 1% NHS in 0.02 M KPBS for 48 hours at 4°C. Following incubation in the primary antiserum, sections were washed 3 × 10 minutes in 0.02 M KPBS containing 2% NHS. Sections were then incubated in a solution containing horse biotinylated antimouse IgG (1:227; Vector Laboratories, Cat. no. BA-2000), 1% NHS, and 0.3% TX-100 in 0.02 M KPBS one hour at room temperature, washed 3 × 5 minutes in 0.02 M KPBS, and incubated for 45 minutes at room temperature in avidin-biotinylated HRP solution (Biostain ABC kit, Biomeda, Cat. no. 11-001) in 0.02 M KPBS. Sections were then washed 3 × 10 minutes in 0.02 M KPBS, incubated in secondary antibody solution for another 45 minutes, washed 3 × 10 minutes in 0.02 M KPBS (no NHS), incubated in the avidin-biotin complex solution for 30 minutes, washed 1 × 10 minutes in 0.02 M KPBS and 2 × 10 minutes in 0.05 M Tris buffer, incubated for 30 minutes in a solution containing 0.05% diaminobenzidine (DAB, Sigma-Aldrich, Cat. no. D9015-100mg), and 0.04% H_2O_2 in 0.05 M Tris buffer, washed 3 × 10 minutes, mounted on gelatin-coated slides, air-dried overnight, defatted, hydrated, and intensified with the silver nitrate-gold chloride method described above.

Calbindin-D_{28K}

The procedure for visualizing calbindin-positive fibers and cell bodies was carried out on free-floating sections using a mouse anti-calbindin-D_{28K} monoclonal antibody (SWANT, Cat. no. 300, lot 18F). This antibody is a mouse IgG produced by hybridization of mouse myeloma cells with spleen cells from mice immunized with calbindin-D_{28K} purified from chicken gut. The antibody specifically stains the ^{45}calcium-binding spot of calbindin-D_{28K} (MW 28,000, IEF 4.8) in a two-dimensional gel. In radioimmunoassay it detects calbindin D_{-28K} with a sensitivity of 10 ng/assay and an affinity of 1.6×10^{12} L/M (SWANT). Staining patterns were comparable to those previously described in primates (see Results and Discussion sections for detailed description, comparison, and references). Sections that had been maintained in TCS at –70°C were washed 3 × 10 minutes in 0.02 M KPBS (pH 7.4). To eliminate endogenous peroxidase activity, sections were treated with 1% H_2O_2 in dH_2O for 15 minutes after which the sections were rinsed 6 × 5 minutes in 0.02 M KPBS. To block nonspecific binding, sections were incubated in a solution containing 10% NHS (Biogenesis, Cat. no. 8270-1004) and 0.5% TX-100 in 0.02 M KPBS for 4 hours at room temperature. Sections were then incubated with the mouse anti-calbindin-D_{28K} monoclonal antibody (1:5,000) in 0.5% TX-100 and 1% NHS in 0.02 M KPBS for 48 hours at 4°C. Following the 2-day incubation in primary antiserum, sections were washed 3 × 10 minutes in 0.02 M KPBS containing 2% NHS, and incubated in a solution containing horse biotinylated antimouse IgG (1:227; Vector Laboratories, Cat. no. BA-2000), 1% NHS, and 0.3% TX-100 in 0.02 M KPBS (pH 7.4) for 1 hour at room temperature. The sections were then washed 3 × 10 minutes in KPBS and incubated for 45 minutes at room temperature in avidin-biotinylated HRP solution (Biostain ABC kit, Biomeda, Cat. no. 11-001) in 0.02 M KPBS. Sections were then washed 3 × 10 minutes in KPBS, incubated in the secondary antibody solution, washed 3 × 10 minutes in KPBS, and incubated in the avidin-biotin complex solution for 30 minutes. The sections were then washed 1 × 10 minutes in 0.02 M KPBS and 2 × 10 minutes in 0.05 M Tris, and treated with diaminobenzidine (DAB, Sigma-Aldrich, Cat. no. D9015-100mg; 0.05% DAB and 0.04% H_2O_2 in 0.05 M Tris), washed 3 × 10 minutes, mounted on gelatin-coated slides, air-dried overnight, defatted, hydrated, and intensified with the silver nitrate-gold chloride method described above.

Calretinin

The procedure for visualizing calretinin-positive fibers and cell bodies was carried out on free-floating sections using a mouse anti-calretinin monoclonal antibody (SWANT, Cat. no. 6B3, lot 010399). This antibody was raised in mouse by immunization with recombinant human calretinin-22k. Calretinin-22k is an alternative splice product of the calretinin gene and identical to calretinin up to Arg178. After fusion, hybridoma cells were screened with human recombinant calretinin as target, the clone 6B3 was selected, and ascites was produced. The antibody 6B3 recognizes an epitope within the first four EF-hands domains common to both calretinin and calretinin-22k (Zimmermann and Schwaller, 2002). This antibody does not crossreact with calbindin-D_{28K} or other known calcium binding-proteins, as determined by immunoblots (SWANT). Staining patterns were comparable to those previously described in primates (see Results and Discussion sections for detailed description, comparison, and references). Sections that had been maintained in TCS at –70°C were washed 3 × 10 minutes in 0.02 M KPBS (pH 7.4). To eliminate endogenous peroxidase activity, sections were treated with 1% H_2O_2 in dH_2O for 15 minutes, after which the sections were rinsed 6 × 5 minutes in 0.02 M KPBS. To block nonspecific binding the sections were incubated in a solution containing 10% NHS (Biogenesis, Cat. no. 8270-1004) and 0.5% TX-100 in 0.02 M KPBS for 4 hours at room temperature. Sections were then incubated with the mouse anti-calretinin monoclonal antibody (1:5,000) in 0.5% TX-100 and 1% NHS in 0.02 M KPBS for 48 hours at 4°C. Following incubation in the primary antiserum, sections were washed 3 × 10 minutes in 0.02 M KPBS containing 2% NHS, and then incubated in a solution containing horse biotinylated antimouse IgG (1:227; Vector Laboratories, Cat. no. BA-2000), 1% NHS and 0.3% TX-100 in 0.02 M KPBS, (pH 7.4) for

TABLE 2. Summary of Immunohistochemical Procedures Used in the Study

	Primary antibody	Secondary antibody	Blocking serum	Buffer/visualization
Neurofilaments	Monoclonal SMI-32 Sternberger, Cat. no. SMI-32	Horse anti-mouse IgG Vector; Cat. no. BA-2000	NHS, Biogenesis Cat. no. 8270-1004	Tris Avidin-biotin
AChE	Monocolonal anti-AChE Abcam, Cat. no. ab2803-200	Horse anti-mouse IgG Vector; Cat. no. BA-2000	NHS, Biogenesis Cat. no. 8270-1004	KPBS Avidin-biotin
Serotonin	Polyclonal anti-5-HT Diasorin, Cat. no. 20080	Goat anti-rabbit IgG Vector; Cat. no. AI-1000	NGS, Biogenesis Cat. no. 8270-1204	PBS PAP
Parvalbumin	Monoclonal anti-parvalbumin SWANT, Cat. no. 235	Horse anti-mouse IgG Vector; Cat. no. BA-2000	NHS, Biogenesis Cat. no. 8270-1004	KPBS Avidin-biotin
Calbindin-D_{28K}	Monoclonal anti-calbindin SWANT, Cat. no. 300	Horse anti-mouse IgG Vector; Cat. no. BA-2000	NHS, Biogenesis Cat. no. 8270-1004	KPBS Avidin-biotin
Calretinin	Monoclonal anti-calretinin SWANT, Cat. no. 6B3	Horse anti-mouse IgG Vector; Cat. no. BA-2000	NHS, Biogenesis Cat. no. 8270-1004	KPBS Avidin-biotin
Somatostatin	Polyclonal anti-$SS28_{1-12}$ Gift of Dr. Robert Benoit	Goat anti-rabbit IgG Vector; Cat. no. AI-1000	NGS, Biogenesis Cat. no. 8270-1204	KPBS Avidin-biotin

1 hour at room temperature. Sections were washed 3 × 10 minutes in 0.02 M KPBS and incubated for 45 minutes at room temperature in avidin-biotinylated HRP solution (Biostain ABC kit, Biomeda, Cat. no. 11-001) in 0.02 M KPBS. Sections were then washed 3 × 10 minutes in KPBS, incubated for 45 minutes in the secondary antibody solution, washed 3 × 10 minutes in KPBS, and incubated in the avidin-biotin complex solution for 30 minutes. Sections were then washed 1 × 10 minutes in 0.02 M KPBS and 2 × 10 minutes in 0.05 M Tris buffer, and treated with diaminobenzidine (DAB, Sigma-Aldrich Chemicals, Cat. no. D9015-100mg; 0.05% DAB and 0.04% H_2O_2 in 0.05M Tris), washed 3 × 10 minutes in KPBS, mounted on gelatin-coated slides, dried overnight, defatted, hydrated, and intensified with the silver nitrate–gold chloride method described above.

Somatostatin

The procedure for visualizing somatostatin immunoreactivity was carried out on free-floating sections using a rabbit anti-somatostatin $SS28_{1-12}$ (anti-$SS28_{1-12}$) polyclonal antibody (primary antiserum S320 kindly donated by Dr. Robert Benoit). This antiserum was obtained from rabbits inoculated with somatostatin 28-Tyr conjugated to BSA, and its biochemical and immunohistochemical specificity has been previously characterized (Benoit et al., 1982a,b). Serum S320 has an antigenic determinant that corresponds to the last eight amino acids of SS28, i.e., $SS28_{1-12}$, and shows no crossreactivity with SS28. The specificity of the antiserum for detecting $SS28_{1-12}$ in the monkey hippocampal formation has been previously demonstrated by the absence of labeling following incubation of the antiserum with 5 or 10 nmol/mL of $SS28_{1-12}$ (Bakst et al., 1985). Sections that had been maintained in TCS at –70°C were rinsed 3 × 10 minutes in 0.02 M KPBS (pH 7.4), treated against endogenous peroxidase by immersion in 0.5% hydrogen peroxide solution in 0.02 M KPBS for 15 minutes, and rinsed 6 × 5 minutes in 0.02 M KPBS. Sections were then incubated for 4 hours in a blocking solution made of 0.5% TX-100, 5% normal goat serum (NGS; Biogenesis, Cat. no. 8270-1204) in 0.02 M KPBS at room temperature. Sections were then incubated overnight with the rabbit anti-$SS28_{1-12}$ polyclonal antibody (1:5,000) in 0.5% Triton X-100, 5% NGS in 0.02 M KPBS at 4°C with rotation. Sections were then washed 3 × 10 minutes in 0.02 M KPBS with 2% NGS, incubated for 1 hour with a secondary antibody, biotinylated goat antirabbit IgG (1:100; Vector Laboratories, Cat. no. AI-1000) in 0.3% Triton X-100, 2% NGS in 0.02 M KPBS, rinsed 3 × 10 minutes in 0.02 M KPBS with 2% NGS, incubated for 45 minutes in an avidin-biotin complex solution (Biostain ABC kit, Biomeda, Cat. no. 11-001), washed 3 × 10 minutes in 0.02 M KPBS, incubated in secondary antibody solution for another 45 minutes, washed 3 × 10 minutes 0.02 M KPBS (no NGS), incubated in the avidin-biotin complex solution for 30 minutes, washed 3 × 10 minutes in 0.05 M Tris buffer, incubated for 30 minutes in a solution containing 0.05% diaminobenzidine (DAB, Sigma-Aldrich, Cat. no. D9015-100mg), 0.04% H_2O_2 in 0.05 M Tris buffer, and washed 3 × 10 minutes. Sections were then mounted on gelatin-coated slides from filtered 0.05 M PB and air-dried overnight at 37°C. Reaction product was then intensified with the silver nitrate–gold chloride method described above.

Control staining procedures

Following the suggestions by Saper and Sawchenko (2003) and Holmseth et al. (2006), we performed a number of verifications to control for the specificity of the immunostaining procedures used in this study (Table 2). First, we processed a series of sections omitting the primary antibody. Second, we used several primary antibodies directed toward different antigens with non-overlapping distributions. Because the antibodies employed in this study have been used previously and their patterns of immunoreactivity well characterized in perfusion-fixed monkey tissue, we did not perform additional controls (e.g., such as preadsorption with the peptides used to generate the antibody). Where appropriate, we refer to earlier publications demonstrating the specificity of each antiserum.

Photomicrograph production

Low-magnification photomicrographs were taken with a Leica DFC420 digital camera on a Leica MZ9.5 stereomicroscope (Leica Microsystems, Wetzlar, Germany). High-magnification photomicrographs were taken with a Microfire S99808 digital camera (Optronics, Goleta, CA) on a Nikon Eclipse 80i microscope (Nikon Instruments, Tokyo, Japan). Artifacts located outside the sections were removed, and levels were adjusted in Adobe Photoshop CS, v. 8.0 (Adobe, San Jose, CA).

RESULTS

Nissl stain

Perfused tissue. The hippocampal formation comprises the dentate gyrus, the hippocampus proper, the subiculum, the presubiculum, the parasubiculum, and the entorhinal cortex (Fig. 1) (Lavenex and Amaral, 2000). We refer the reader to our previous descriptions of the nomenclature, cytoarchitectonic organization, and boundaries of the monkey hippocampal formation in perfused, Nissl-stained preparations (Pit-

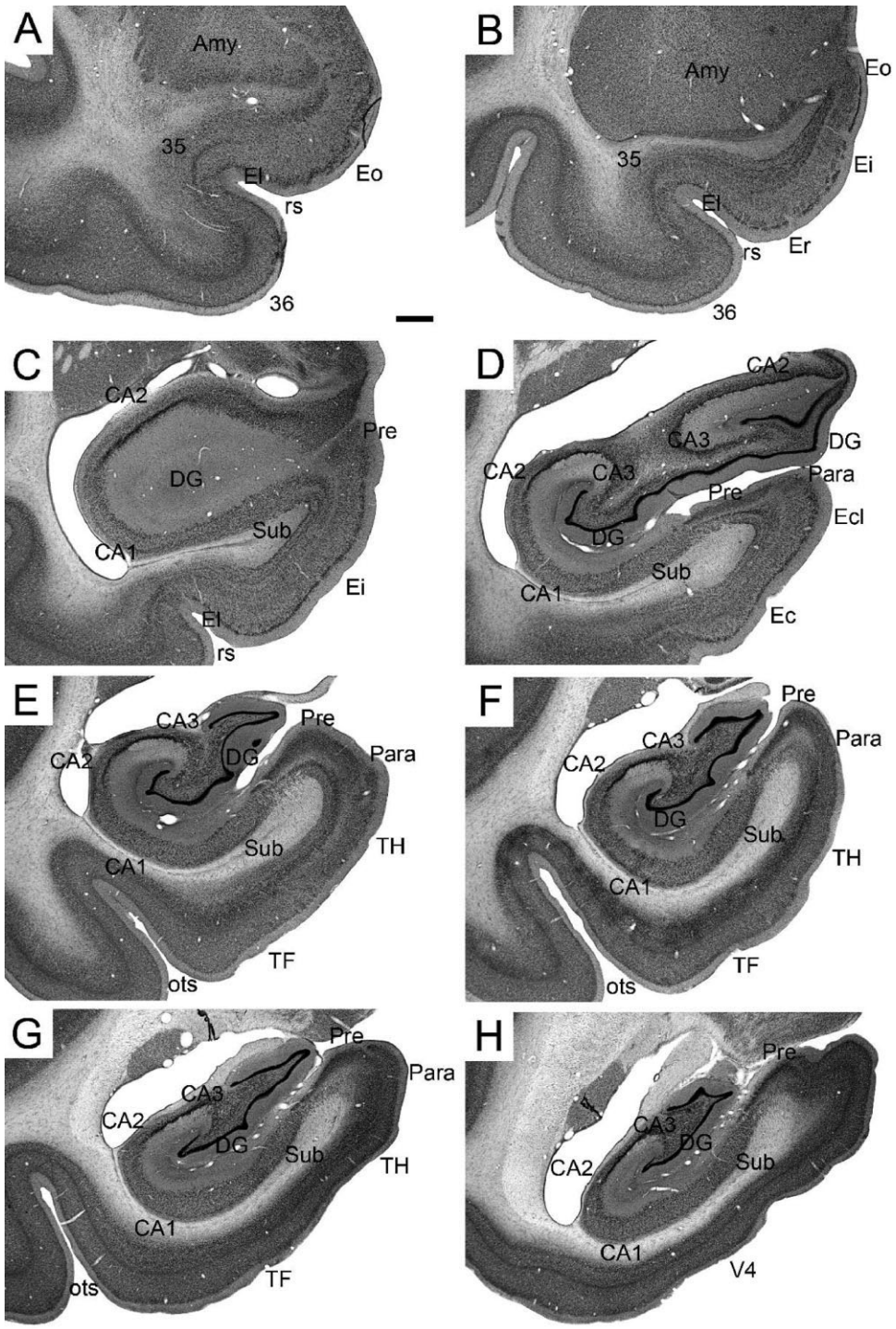

Figure 1.
Low-magnification photomicrographs of Nissl-stained coronal sections through the monkey hippocampal formation. Sequential panels are separated by 2.4 mm and arranged from rostral **(A)** to caudal **(H)**. Amy: amygdala; CA1: CA1 field of the hippocampus; CA2: CA2 field of the hippocampus; CA3: CA3 field of the hippocampus; DG: dentate gyrus; Ec: caudal division of the entorhinal cortex; Ecl: caudal limiting division of the entorhinal cortex; Ei: intermediate division of the entorhinal cortex; El: lateral division of the entorhinal cortex; Eo: olfactory division of the entorhinal cortex; Er: rostral division of the entorhinal cortex; ots: occipito-temporal sulcus; Para: parasubiculum; Pre: presubiculum; rs rhinal sulcus; Sub: subiculum; TF: area TF of the parahippocampal cortex; TH: area TH of the parahippocampal cortex; V4: area V4 of the primary visual cortex; 35: area 35 of the perirhinal cortex; 36: area 36 of the perirhinal cortex. Scale bar = 1 mm in A (applies to all).

TABLE 3. Measurements of Morphological Characteristics in Nissl-Stained Preparations

	DG granule cell size		CA1 pyramidal cell size		LGN neuron size		Brain volume extrapolation	
	Median	Mean	Median	Mean	Median	Mean	Median	Mean
Perfused (n = 10)	617 ± 24	663 ± 32	4099 ± 170	4282 ± 181	1711 ± 126	1780 ± 133	54.5	55.3
Immersed (n = 10)	228 ± 13	245 ± 13	2888 ± 167	3154 ± 186	1035 ± 50	1023 ± 118	73.0	70.1
Average Perf & Imm	423 ± 47	454 ± 51	3494 ± 181	3718 ± 181	1391 ± 103	1421 ± 123		
Ratio (Perf/Imm)	2.70	2.70	1.42	1.36	1.65	1.74	0.75	0.79

Cell size in μm^3 ± SD, brain volume in mm^3.

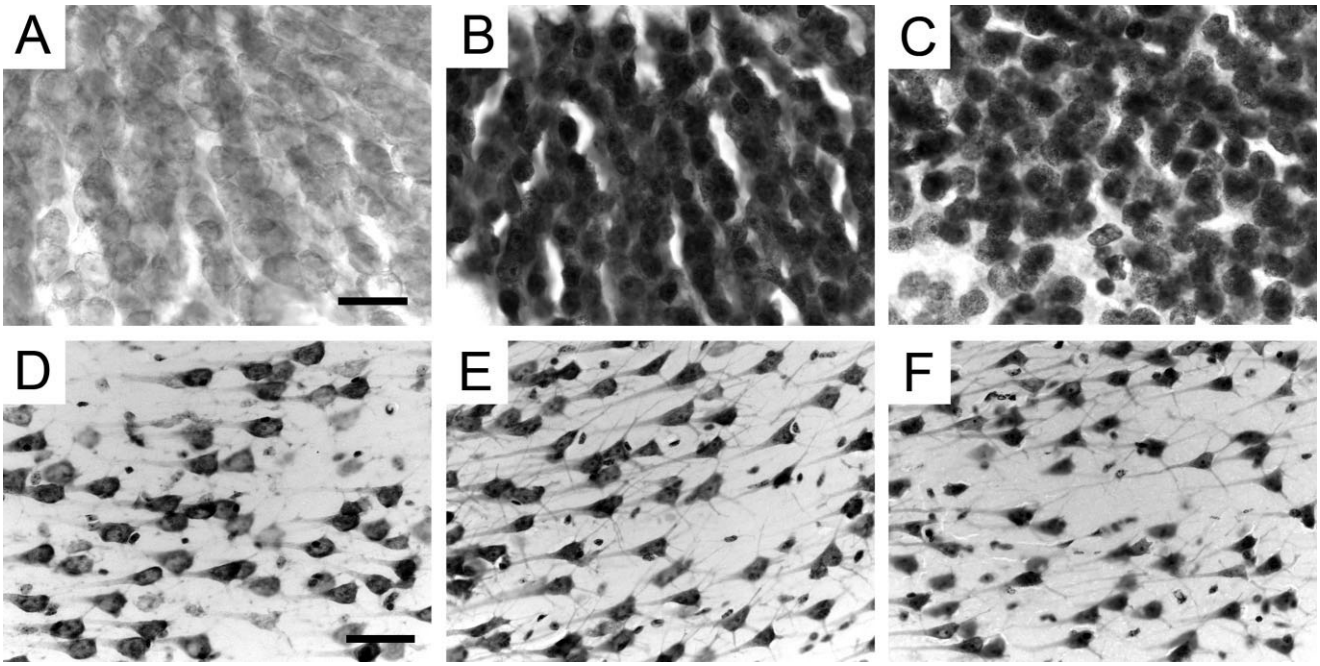

Figure 2.
High-magnification photomicrographs of Nissl-stained neurons in the monkey hippocampal formation. **A–C:** Granule cells of the dentate gyrus. A: PM-15-03, perfusion-fixed. B: PM-10-02, immersion-fixed 2 hours postmortem. C: PM-04-02, immersion-fixed 48 hours postmortem. Note the decreased soma size and increased staining intensity of dentate granule cells in immersion-fixed tissue. **D–F:** Pyramidal neurons in the CA1 field of the hippocampus. D: PM-15-03, perfusion-fixed. E: PM-03-02, immersion-fixed 2 hours postmortem. F: PM-02-02, immersion-fixed 48 hours postmortem. Note the decreased soma size and increased dendritic labeling of CA1 pyramidal neurons in immersion-fixed tissue. Scale bars = 20 μm in A (applies to B,C); 50 μm in D (applies to E,F).

känen and Amaral, 1993b; Kobayashi and Amaral, 1999; Amaral and Lavenex, 2007).

Immersion-fixed tissue. Analysis of Nissl-stained sections through the hippocampal formation of adult monkey brains fixed by immersion in 4% PFA after various postmortem intervals revealed striking differences with the patterns observed in brains from monkeys perfused transcardially with the same fixative. First, at low magnification overall brain volume was larger in immersion-fixed tissue. We extrapolated the volumetric changes observed in total brain volume (Table 3) from measurements of the surface area of a coronally cut section located at the mid-rostrocaudal level of the hippocampus using the algebraic formula to determine the volume of a sphere: brain volume = 4/3 * surface area * (sqrt-[surface area/3.1416]). Total extrapolated brain volume was about 25% larger in brains fixed by immersion than in perfusion-fixed brains. An unexpected contrast to increased brain volume, however, was the finding that neuronal soma volume decreased with immersion-fixation as compared to perfusion-fixation. Moreover, the degree of shrinkage varied depending on the neuronal population considered (Table 3). Soma volume was 63% smaller for the granule cells of the dentate gyrus, but only 26% smaller for the CA1 pyramidal neurons. It was therefore impossible to predict the differences in neuronal soma size between perfusion- and immersion-fixed tissue in various brain areas. For example, estimates conducted for principal neurons of the lateral geniculate nucleus revealed a soma size 40% smaller in immersion-fixed tissue.

There were also clear qualitative differences in Nissl staining between fixation methods. Cell somas were generally more darkly stained in immersion-fixed tissue (Fig. 2). Interestingly, although our analyses did not show that soma size was further affected by increasing postmortem intervals, the general appearance of neurons and principal cell layers exhibited consistent variations. In the densely packed granule cell layer of the dentate gyrus, cell somas were more spherical in immersion-fixed preparations and

could be more easily distinguished from each other, particularly at longer postmortem intervals (Fig. 2B,C). Similarly, the dendrites of CA1 pyramidal cells were more clearly stained in immersion-fixed tissue, and soma shape was more pyramidal than in perfused tissue, in which they appeared more spherical (Fig. 2D–F).

Nonphosphorylated high-molecular-weight neurofilaments

Perfused tissue. Analysis of SMI-32 immunoreactivity patterns in the hippocampal formation of perfused monkeys revealed high levels of expression of nonphosphorylated high-molecular-weight neurofilaments (NF-H) in CA3, CA2, the subiculum, and the entorhinal cortex (Fig. 3) (Siegel et al., 1993; Lavenex et al., 2004a). Microscopic analysis revealed that in all regions heavy labeling was largely restricted to dendritic processes, whereas cell body labeling was only light to moderate. Nonphosphorylated NF-H expression was detected in the cell bodies and dendrites of neurons within the polymorphic layer of the dentate gyrus. In some cases the dendrites of these neurons extended into the molecular layer. Although the dendrites and somas of the granule cells did not exhibit detectable levels of expression of the protein, punctate labeling was visible in the inner molecular layer. Inconsistently, the mossy fiber pathway exhibited light labeling in its proximal portion (within the blades of the dentate gyrus), but not at the level of the end bulb. In the distal portion of CA3 and in CA2 there was a high level of expression of nonphosphorylated NF-H in the basal dendrites of pyramidal cells extending into stratum oriens, as well as in the apical dendrites extending into stratum radiatum. Nonphosphorylated NF-H were highly expressed in some fusiform neurons located in stratum oriens of CA3, CA2, and CA1. The somas of CA1 pyramidal cells were faintly labeled, but there was no detectable expression in stratum lacunosum moleculare. In the subiculum, there was a high level of expression of nonphosphorylated NF-H throughout the pyramidal cell layer and the deep portion of the molecular layer; cell bodies were moderately labeled, whereas dendrites were heavily labeled. Layer I of the presubiculum was largely unstained, whereas the superficial portion of layer II contained moderately labeled fibers and cells bodies. In the entorhinal cortex the highest level of expression was detected in layer II, particularly within the cell islands of the intermediate division (Ei). Cell bodies were lightly to moderately labeled, whereas dendrites were heavily labeled. Layers V and VI contained moderately to heavily labeled dendrites, with lightly to moderately labeled cell bodies. Dendritic processes in layer III were only faintly labeled, with the exception of a few isolated, heavily labeled neurons. There was no detectable expression in layer I. No other layer or subdivision of the adult monkey hippocampal formation expressed detectable levels of nonphosphorylated NF-H.

Immersion-fixed tissue. Analysis of SMI-32 immunoreactivity patterns in the hippocampal formation of immersion-fixed brains revealed striking differences with the patterns observed in perfusion-fixed brains (Fig. 3), but no differences due to the varying postmortem intervals until immersion-fixation (i.e., patterns of staining in tissue immersion-fixed after 2 hours resembled those in tissue immersion-fixed after 48 hours). In immersion-fixed tissue, staining in the entorhinal cortex exhibited a strong rostrocaudal variation in staining intensity. Whereas reactivity was drastically reduced, and in some cases totally absent, in the rostral entorhinal cortex (Fig. 3C,D), significant staining often remained in the caudal entorhinal cortex (not shown). Interestingly, however, layer V of the entorhinal cortex was conspicuously unstained even in the caudal regions of immersion-fixed tissue. In contrast, mossy fiber axons were more heavily stained than in perfused tissue (3E,F). Nonphosphorylated NF-H immunoreactivity was also greatly reduced in the somas and dendrites of neurons located in the polymorphic layer of the dentate gyrus. In some cases, staining intensity was also reduced in CA3 and CA2 pyramidal neurons. In contrast, fusiform neurons in stratum oriens of CA3, CA2, and CA1 were intensely labeled in immersion-fixed tissue. Finally, in the presubiculum of immersion-fixed tissue, SMI-32 immunoreactivity was drastically reduced, if not completely absent.

Acetylcholinesterase

Perfused tissue. The pattern of acetylcholinesterase (AChE) innervation in the rhesus monkey (*Macaca mulatta*) hippocampal formation largely resembled that previously described by Bakst and Amaral (1984) in the cynomolgus monkey (*Macaca fascicularis*). Our description is based mainly on the observation of material prepared for the visualization of AChE enzymatic activity (Fig. 4). However, we briefly discuss a few significant differences observed in tissue prepared by the immunohistochemical method for AChE visualization.

In the dentate gyrus there was intense diffuse staining of the inner one-third of the molecular layer. Staining intensity was greatest at rostral levels and progressively decreased caudally. There was a distinctly denser band of staining just above and partly within the superficial margin of the granule cell layer. Even though it was difficult to observe through the diffuse precipitate in the inner molecular layer, fiber staining appeared largely homogenous across the depth of the molecular layer with the exception of a slightly higher fiber density in the outer one-third of the layer. The granule cells were unstained but there were AChE-positive fibers running through the granule cell layer. The polymorphic layer of the dentate gyrus had a narrow band of heavy staining (which corresponds to an acellular layer in Nissl-stained sections) just subjacent to the granule cell layer. The remainder of the polymorphic layer was less intensely stained and at caudal levels almost entirely unstained.

In CA3 there was intense staining of the stratum oriens, which extended into the pyramidal cell layer. By contrast, most of the alveus and the pyramidal cell somas were largely unstained. Stained fibers ran mostly perpendicular through stratum lucidum. Staining was moderate to heavy in stratum radiatum with a distinct thin band of heavier staining at the deep margin of stratum radiatum. Stratum lacunosum-moleculare exhibited heavy fiber staining, which contrasted greatly with that observed in CA1 (see below). CA2 was heavily stained, especially in the caudal part of the hippocampus. In fact, the densest zone of labeling along the transverse axis of the hippocampus appeared to shift from distal CA3 to CA2 as one progressed from rostral to caudal along the long axis of the hippocampus. This heavy staining contrasted markedly with CA1, which was more lightly stained than CA3 and CA2. Stratum oriens and stratum radiatum of CA1 had a more evenly distributed pattern of staining, though the intensity of staining increased sharply at the border with the subiculum. Stratum lacunosum-moleculare was lightly stained

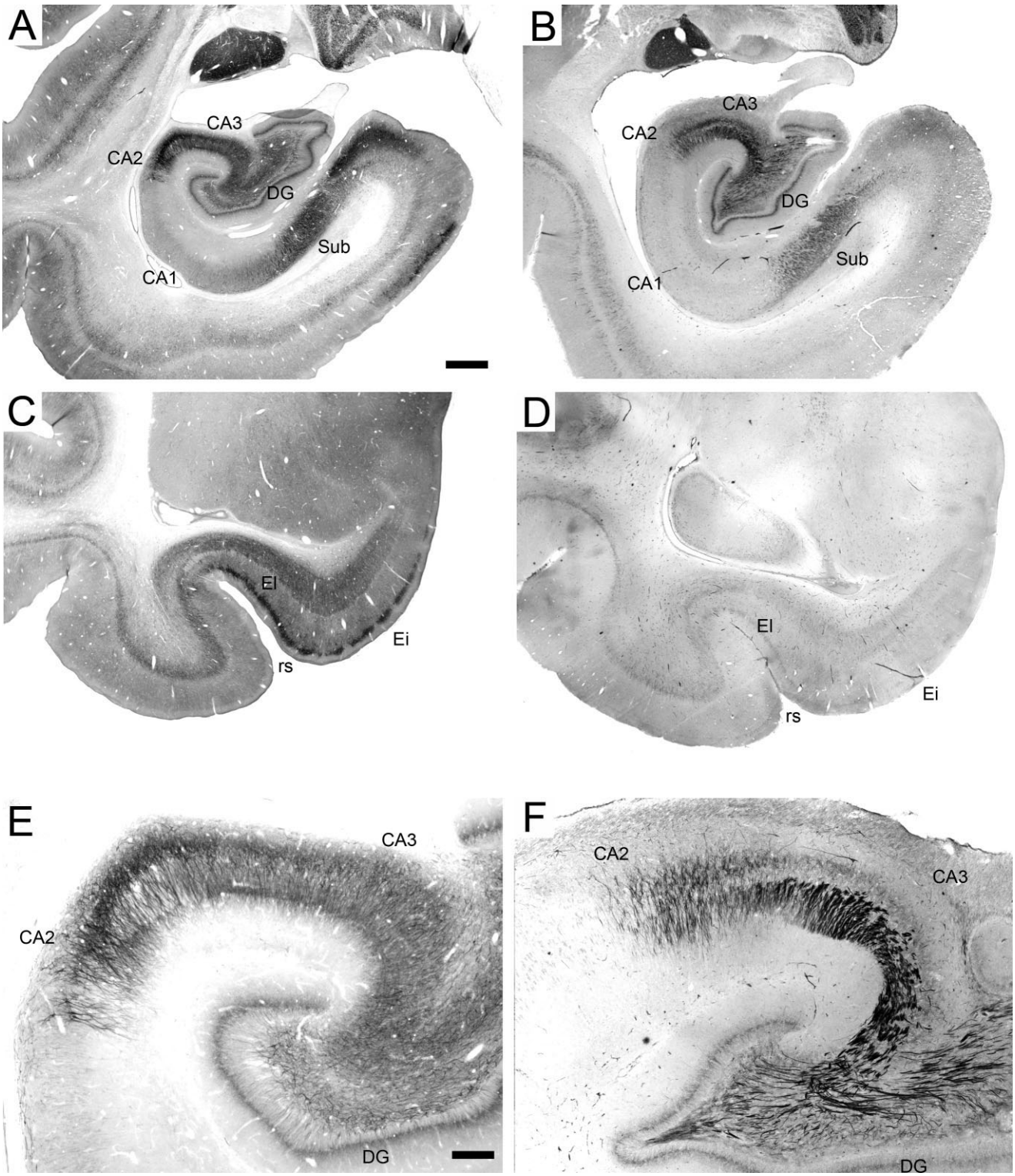

Figure 3.
Nonphosphorylated high-molecular-weight neurofilament (SMI-32) immunoreactivity in the monkey hippocampal formation **(A,B)**. A: PM-15-03, perfusion-fixed. B: PM-04-02, immersion-fixed 48 hours postmortem. **C,D:** Intermediate division of the entorhinal cortex. C: PM-15-03, perfusion-fixed. D: PM-03-02, immersion-fixed 2 hours postmortem. **E,F:** CA3 field of the hippocampus. E: PM-15-03, perfusion-fixed. F: PM-03-02, immersion-fixed 2 hours postmortem. Note the absence of staining in the entorhinal cortex and the increased staining of the mossy fiber pathway in immersion-fixed tissue. For abbreviations, see Fig. 1. Scale bars = 1 mm in A (applies to B–D); 250 μm in E (applies to F).

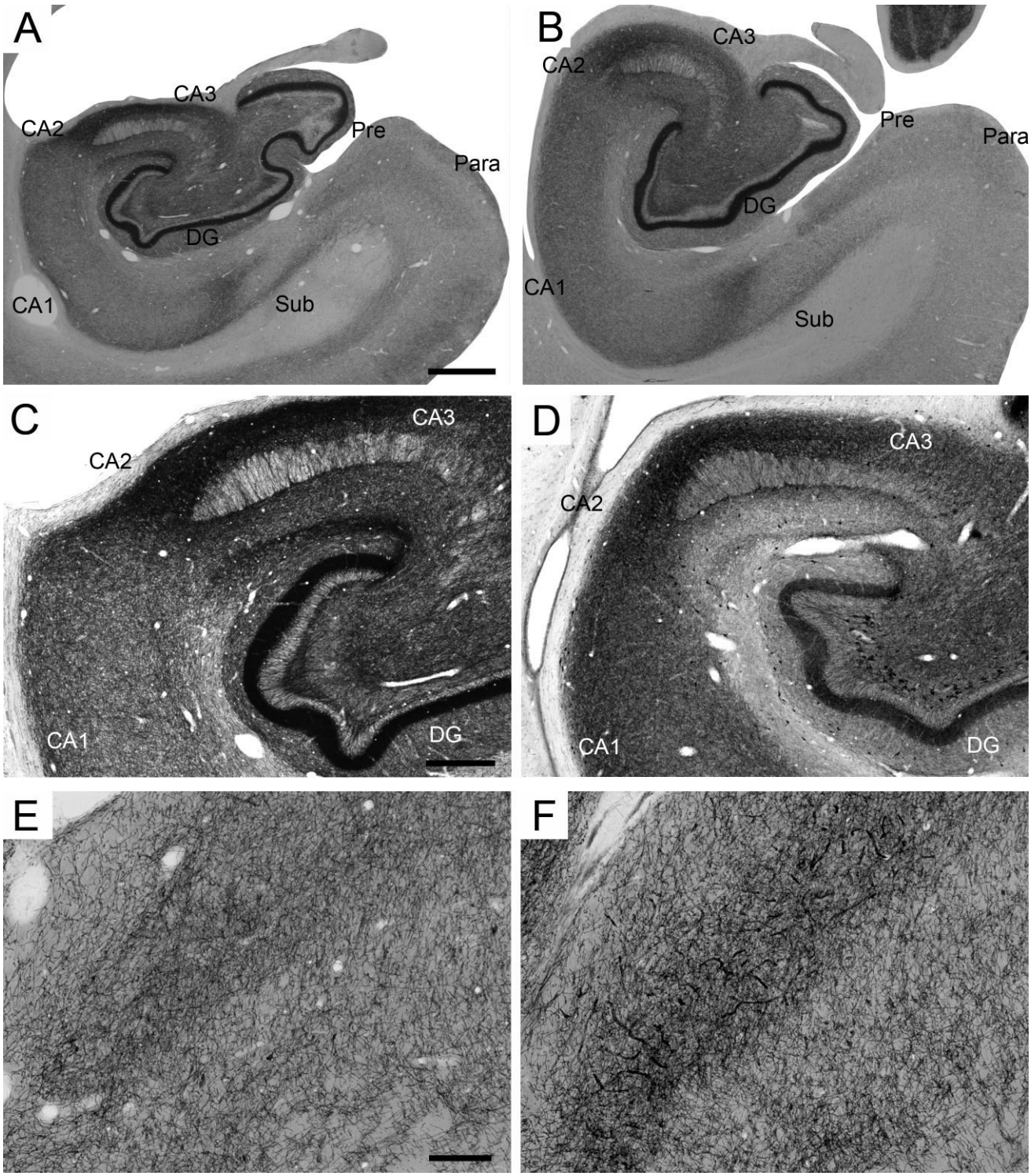

Figure 4.
Acetylcholinesterase (AChE) distribution in the monkey hippocampal formation. **A,B:** Low-magnification photomicrographs of the AChE enzymatic activity. A: PM-15-03, perfusion-fixed. B: PM-04-02, immersion-fixed 48 hours postmortem. **C,D:** AChE distribution in the dentate gyrus, CA3, CA2, and CA1 fields of the hippocampus. C: PM-15-03, perfusion-fixed, enzymatic activity. D: PM-15-03, perfusion-fixed, immunohistochemical reactivity. Note the presence of AChE-positive neurons in the polymorphic layer of the dentate gyrus in tissue processed immunohistochemically. **E,F:** AChE enzymatic activity in the presubiculum. E: PM-15-03, perfusion-fixed. F: PM-03-02, immersion-fixed 2 hours postmortem. Note the presence of stained capillaries in the presubiculum of immersion-fixed tissue. For abbreviations, see Fig. 1. Scale bars = 1 mm in A (applies to B); 400 μm in C (applies to D); 150 μm in E (applies to F).

throughout much of the transverse extent of CA1, but there was also a conspicuous patch of heavier staining at the border with the subiculum.

The pyramidal cell layer of the subiculum was lightly but uniformly stained, with the exception of a thin band of slightly heavier staining above the pyramidal cell layer in the molecular layer. Staining in the rest of the molecular layer of the subiculum was similar to that observed in the stratum lacunosum moleculare of CA1. The most distinctive layer of the subiculum in AChE preparations was the deep layer (layer III), which contained numerous stained fibers and cell bodies throughout its rostrocaudal extent.

In the presubiculum, the deep portion of the outer, cell-dense layer II contained a moderately dense plexus of AChE-positive fibers. In contrast, the superficial portion of layer II was more lightly stained. The molecular layer exhibited a rostrocaudal gradient to its staining pattern. Rostrally, the molecular layer was moderately stained, and thus contrasted with the lightly stained superficial portion of layer II. Caudally, however, the molecular layer was much less intensely stained, and basically indistinct from the superficial portion of layer II.

Layer I of the parasubiculum was lightly stained. Layer II was moderately but uniformly stained. In contrast to what was previously reported by Bakst and Amaral (1984) for the cynomolgus monkey, we did not observe any clear topographical arrangement in the two rhesus macaque cases that were perfusion-fixed.

Staining in the rostral portion of the entorhinal cortex (areas Eo and Er) was uniform but diffuse. At more caudal levels (areas Ei, Ec, Ecl), the pattern of staining was more laminar, and layers II, III, and V were distinctly labeled. Interestingly, whereas the lateral half of layer I within the rhinal sulcus (areas Elr and Elc) was moderately, diffusely labeled and had relatively darkly labeled fibers, the medial half of layer I, superjacent to the gyrus, was less intensely diffusely labeled and had more lightly labeled fibers. Our observations of extrahippocampal brain regions confirmed that this phenomenon was not specific to the entorhinal cortex. Indeed, we observed that wherever two cortices abut (i.e., within a sulcus or between the 2 hemispheres), layer I is moderately stained with AChE, and the traversing fibers are darkly stained. In contrast, on gyri, where cortices do not abut, layer I is only lightly stained, and fiber staining is considerably reduced.

Finally, the overall regional pattern of staining was much better defined in perfusion-fixed tissue processed for the visualization of AChE enzymatic activity than in tissue processed immunohistochemically. However, individual AChE-positive fibers were more clearly defined in the immunostained tissue when observed at high magnification (40–100×). Although there was no soma staining in the dentate gyrus of tissue processed for the visualization of the AChE enzymatic activity, in tissue processed with the immunohistochemical method the somas of what appeared to be the mossy cells (located in the polymorphic layer) were heavily stained throughout the entire rostrocaudal extent of the dentate gyrus (Fig. 4C,D).

Immersion-fixed tissue. AChE distribution in the hippocampal formation appeared to be largely unaffected by postmortem interval or immersion-fixation (Fig. 4A,B). There were, however, a few differences. First, the overall staining intensity appeared decreased throughout the brain. Although regional staining patterns remained unchanged, and the density of AChE-positive fibers did not seem to be affected, the staining intensity of individual fibers was weaker. Interestingly, this difference was less detectable in the hippocampal formation, possibly because staining intensity was generally greater than in the rest of the brain (with the result that fibers and areas with diffuse precipitate remained heavily stained).

Second, we observed a light to moderate staining of capillary profiles in layer II of the presubiculum in immersion-fixed tissue treated enzymatically (Fig. 4F). Within the hippocampal formation, this staining pattern was strictly restricted to the presubiculum. However, we also observed the same capillary profiles in layer IV of the retrosplenial cortex (Kobayashi and Amaral, 2000), and in various thalamic nuclei, including the ventral anterior, mediodorsal, ventrolateral nuclei, and the pulvinar. This staining was never observed in tissue processed for the immunohistochemical detection of AChE (Fig. 4E).

Finally, immunostained fibers did not appear any different in immersion-fixed tissue compared to perfusion-fixed tissue. However, there was a large decrease in the intensity of immunostaining of the mossy cell somas in the polymorphic layer of immersion-fixed brains.

Serotonin

Perfused tissue. The pattern of serotonergic innervation in the perfused rhesus monkey hippocampal formation (Fig. 5) largely resembled that previously described in the cynomolgus monkey (Amaral and Campbell, 1986; Kobayashi and Amaral, 1999). In the dentate gyrus there was a moderately dense distribution of 5-HT-immunoreactive fibers in the outer half of the molecular layer and in the polymorphic layer. The density of immunoreactive fibers was substantially lower in the inner half of the molecular layer, and the granule cell layer contained only a few radially oriented 5-HT-immunoreactive fibers.

5-HT-immunoreactive axons and terminals were found throughout the monkey hippocampus (Fig. 5C). Immunoreactive fibers were densest in the stratum lacunosum-moleculare and a moderately dense plexus of serotonin fibers was visible in stratum radiatum, the pyramidal cell layer, and in stratum oriens. In CA3 there seemed to be a gradient in serotonergic innervation along the transverse axis. Fiber density was moderate in the proximal portions of the pyramidal cell layer, strata oriens, and radiatum, and became lighter as one progressed distally. Fiber density was lowest in stratum lucidum and only a few isolated fibers were visible at the level of the end bulb. In CA1 the highest fiber density was found in the deep portion of stratum lacunosum-moleculare. The distribution of 5-HT-immunoreactive fibers was relatively homogeneous within strata oriens, pyramidale, and radiatum. There were, however, two inverse gradients along the transverse axis of CA1. In strata oriens, pyramidale, and radiatum there was a moderate to high 5-HT-immunoreactive fiber density proximally, close to CA2, and a relatively lighter fiber density distally, at the border with the subiculum. In contrast, there was an increase in 5-HT-immunoreactive fiber density from proximal to distal in stratum lacunosum-moleculare. The distribution of 5-HT-immunoreactive fibers in CA2 was largely similar to that observed in proximal CA1.

There was a relatively homogenous, moderate density of serotonergic fibers in the subiculum, although the molecular layer could be distinguished from the pyramidal cell layer by the over-

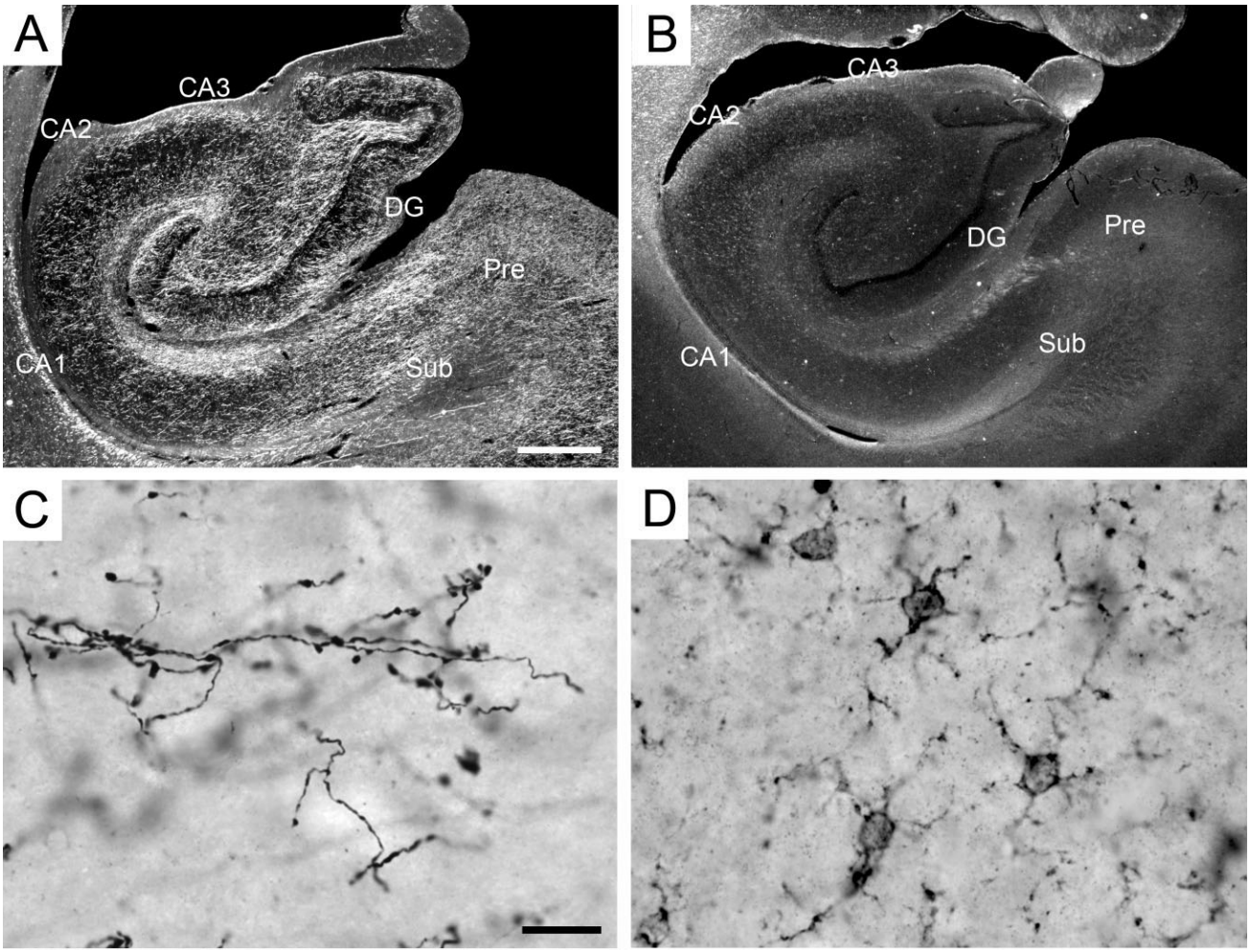

Figure 5.
Serotonin immunoreactivity in the monkey hippocampal formation. **A,B:** Darkfield low-magnification photomicrographs of the distribution of 5-HT-immunoreactive fibers. A: PM-17-03, perfusion-fixed. B: PM-03-02, immersion-fixed 2 hours postmortem. **C,D:** High-magnification photomicrographs of the 5-HT-immunoreactivity in the molecular layer of the dentate gyrus. C: PM-17-03, perfusion-fixed. D: PM-02-02, immersion-fixed 48 hours postmortem. Note the serotonin-positive fibers in perfusion-fixed tissue, but not in immersion-fixed tissue. Note also the presence of immunoreactive microglia in immersion-fixed, but not perfusion-fixed tissue (see text for details). For abbreviations, see Fig. 1. Scale bars = 250 μm in A (applies to B); 15 μm in C (applies to D).

all orientation and shorter length of 5-HT-immunoreactive fibers. There was a dense plexus of 5-HT-immunoreactive fibers in layers I and II of the presubiculum. There was a mediolateral gradient in layer I, with a moderate fiber density proximally (at the border with the subiculum) and a relatively higher density distally. The superficial portion of layer II could easily be distinguished by a slightly lower density of 5-HT-immunoreactive fibers than the rest of the presubiculum. There were few 5-HT-immunoreactive fibers within the parasubiculum.

In the rostral portion of the entorhinal cortex (areas Eo and Er), the distribution of 5-HT-immunoreactive fibers was dense and appeared relatively homogenous across layers. There was, however, a higher density of fibers in Eo, as compared to Er and Elr. Fiber density was lower in the more caudal subdivisions of the entorhinal cortex, but nevertheless, the laminar pattern was distinct.

Immersion-fixed tissue. 5-HT-immunoreactivity was absent in immersion-fixed tissue, even at the shortest postmortem interval of 2 hours (Fig. 5B). Interestingly, large numbers of lightly stained microglia were observed in immersion-fixed tissue (Fig. 5D). Such labeling was never observed in perfusion-fixed tissue (Fig. 5C). However, control immunostaining procedures performed without the primary antibody raised against 5-HT revealed that the microglia staining was in fact due to nonspecific staining by the secondary antibody, goat antirabbit IgG (see also results for somatostatin).

Parvalbumin

Perfused tissue. The pattern of parvalbumin immunoreactivity in the rhesus macaque hippocampal formation (Fig. 6) largely resembled that previously described in the cynomol-

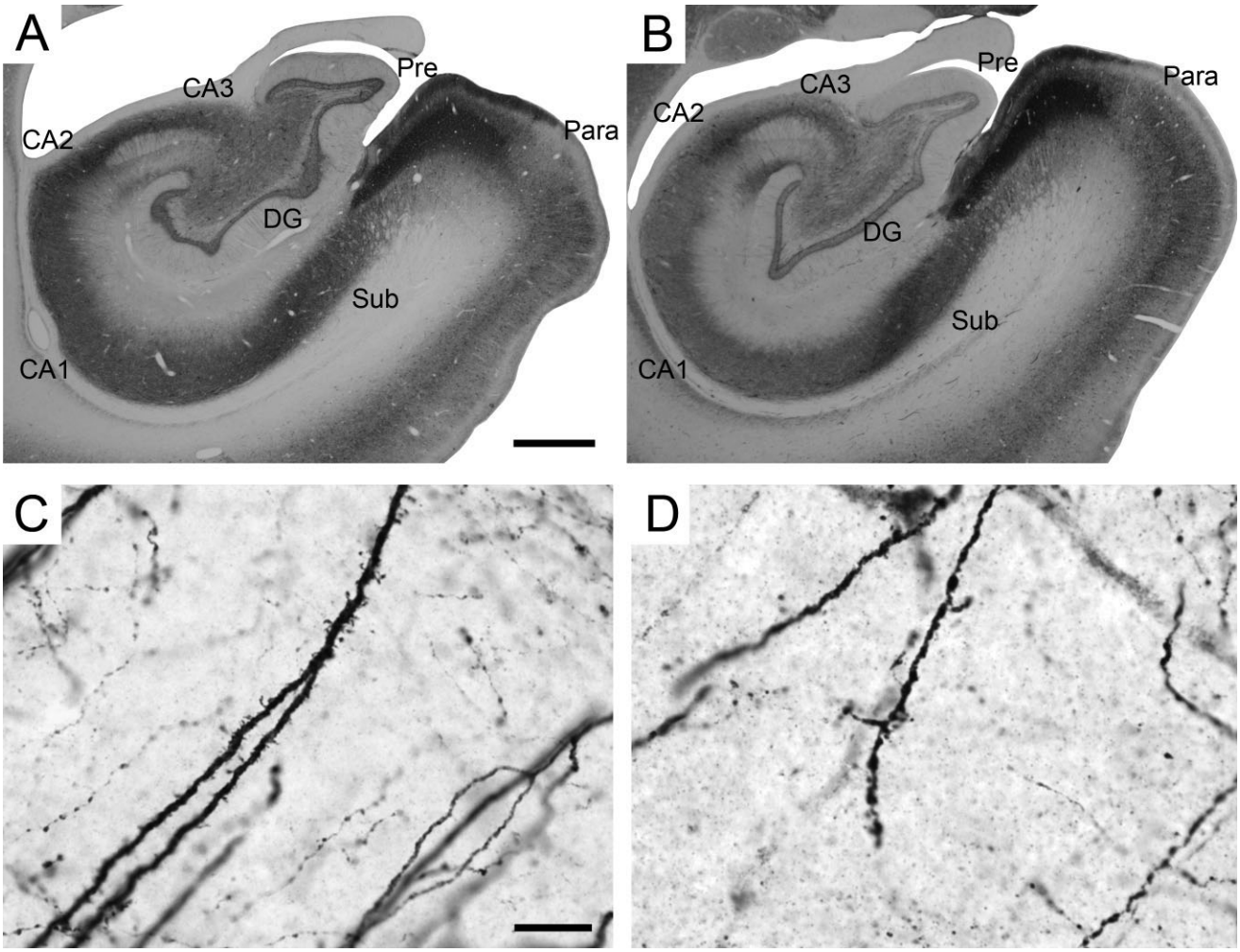

Figure 6.
Parvalbumin immunoreactivity in the monkey hippocampal formation. **A,B:** Low-magnification photomicrographs of the distribution of parvalbumin-immunoreactive fibers and cells. A: PM-15-03, perfusion-fixed. B: PM-03-02, immersion-fixed 2 hours postmortem. **C,D:** High-magnification photomicrographs of parvalbumin-positive fibers in the molecular layer of the dentate gyrus. C: PM15-03, perfusion-fixed. D: PM-04-02, immersion-fixed 48 hours postmortem. Note the absence of visible dendritic spines in immersion-fixed tissue. Abbreviations: see Fig. 1. Scale bars = 1 mm in A (applies to B); 15 μm in C (applies to D).

gus monkey by Pitkänen and Amaral (1993b) and in the rhesus monkey by Seress et al. (1991).

In the dentate gyrus there was a dense pericellular plexus of immunoreactive terminals in the granule cell layer, which outlined the dendrites and cell bodies of unstained neurons. Except for a narrow subgranular zone, there was a marked paucity of terminals in the molecular and polymorphic cell layers. Immunoreactive neurons were mainly located immediately subjacent to the granule cell layer and comprised a variety of morphological cell types, including presumed basket cells. There was also a second zone of increased terminal density at the superficial edge of the granule cell layer. A relatively small number of parvalbumin-immunoreactive cells were present in the molecular layer, and only an occasional labeled cell was observed in the granule cell layer.

The three fields of the hippocampus (CA3, CA2, and CA1) exhibited differences in parvalbumin staining characteristics. In CA3 there was a prominent pericellular terminal plexus in stratum oriens and the pyramidal cell layer that was densest distally (closer to CA2). Parvalbumin-immunoreactive cells were located in stratum oriens or in the pyramidal cell layer, where many had a pyramidal shape and prominent apical and basal dendrites. Parvalbumin-immunoreactive cells in strata lucidum, radiatum, or lacunosum-moleculare were few to none. CA2 had a staining pattern similar to that of CA3, although both the number of labeled cells and the density of the pericellular terminal plexus were greater in CA2. In the CA1 pyramidal cell layer, there were a markedly lower number of parvalbumin-labeled cells than in CA3 and CA2. In contrast, numerous parvalbumin-immunoreactive neurons were found in stratum oriens of CA1. The pyramidal cell layer of CA1 contained a pericellular terminal plexus that was substantially less dense than in CA3 and CA2. There was a marked increase in the number of parvalbumin-

immunoreactive neurons at the border of CA1 and the subiculum.

Parvalbumin-immunoreactive cells were scattered throughout the pyramidal cell layer of the subiculum and comprised a variety of sizes and shapes. Terminal labeling was higher in the pyramidal cell layer of the subiculum than in CA1. Layer II of the presubiculum had one of the highest densities of fiber and terminal labeling in the hippocampal formation, but staining density was slightly lower in the superficial portion of the layer, conveying a tri-laminar appearance. A large number of parvalbumin-immunoreactive cells were scattered throughout layer II of the presubiculum; small, spherical, multipolar cells were commonly observed in layer I. The parasubiculum had an overall lower density of positive cells and fibers than the presubiculum, and their distribution was somewhat more variable than in the presubiculum.

The entorhinal cortex demonstrated striking regional and laminar differences in parvalbumin immunoreactivity. In general, rostral levels of the entorhinal cortex demonstrated lower densities of parvalbumin-immunoreactive fibers and terminals than caudal levels. At any particular level, lateral portions of the field demonstrated more immunoreactive fibers and terminals than medial portions of the field. Throughout the entorhinal cortex, layer III demonstrated the highest density of staining and layer II was somewhat less densely innervated. There were low levels of labeling in layers I, V, and VI, and little or no terminal labeling in layer IV. The distribution of parvalbumin-immunoreactive neurons paralleled the distribution of labeled fibers and terminals.

Immersion-fixed tissue. Although parvalbumin processing was inconsistent in immersion-fixed tissue, and good staining was difficult to achieve, when parvalbumin immunoreactivity was homogeneous it appeared largely similar to that of perfused tissue, at least when viewed at low magnification (4×; Fig. 6B). However, subtle differences were found when these preparations were observed at higher magnification (40 or 100×). Cell bodies and thick dendrites remained heavily stained and labeling quality was not different from perfusion-fixed tissue. In contrast, fine dendritic processes were not as clearly defined; staining was coarser and the definition of spines and filopodial extensions, which could easily be seen in perfused tissue, were not clearly visible or completely absent in immersion-fixed tissue. (Fig. 6C,D).

Calbindin-D_{28K}

Perfused tissue. The pattern of calbindin immunoreactivity we observed in this study (Fig. 7) largely corresponded to that previously described by Seress et al. (1991). Calbindin immunoreactivity was present in all granule cells and in a large proportion of CA2 and CA1 pyramidal neurons, as well as in a distinct population of local circuit neurons in CA3. In the dentate gyrus, calbindin-immunoreactive neurons were also present in the molecular and polymorphic layers, but they did not include the pyramidal basket cells at the polymorphic-granule cell layer border. Instead, the cells in the polymorphic layer tended to be small, bipolar, and located close to the granule cell layer. In the molecular layer, calbindin-D_{28K}-immunoreactive cells were mostly small and scattered, although some other, mostly fusiform cells, were located just adjacent to the hippocampal fissure. Finally, the mossy fibers were highly stained, indeed so darkly stained that preparations for calbindin resemble Timm-stained sections (Amaral and Lavenex, 2007).

In the hippocampus, calbindin-positive nonpyramidal neurons were more frequent in CA3 than in any other part of the hippocampal formation. They were concentrated in the strata oriens and pyramidale of CA3, CA2, and CA1, whereas only a few small neurons were found in the strata lucidum and radiatum of CA3 and in the stratum moleculare of CA1. Most of the positive neurons in stratum oriens were large cells with long dendrites running parallel to the layer. Most cells located in other layers were small with thin, varicose dendrites.

The pyramidal neurons of the subiculum were completely devoid of staining, so that calbindin clearly delineated the CA1-subiculum border. In the presubiculum, layer I and the deeper portion of layer II had a dark neuropil staining, while the superficial portion of layer II appeared unstained. A few small calbindin-positive cells were scattered throughout layer II. The neuropil of the parasubiculum was uniformly moderately stained, and numerous small calbindin-positive cells were distributed throughout layer II of the parasubiculum.

The entorhinal cortex exhibited a striking gradient of calbindin staining. The most rostral and medial portions were strongly labeled, whereas caudal and lateral areas exhibited only weak labeling (Suzuki and Porteros, 2002). This pattern was opposite to that observed for parvalbumin-immunoreactive staining. In all areas, the highest density of calbindin-positive cells and fibers was observed in superficial layers with lower densities in deep layers. Although rostral areas Eo and Er exhibited high densities of calbindin-immunoreactive cells, fibers, and neuropil, calbindin staining gradually decreased in area Ei and was the lowest in caudal areas Ec and Ecl. The rostral half of the entorhinal cortex exhibited a prominent mediolateral gradient. Areas Eo, and the medial portion of areas Er and Ei, were the most strongly stained, and staining decreased as one moved laterally in these fields and was lowest in area El. Caudal areas Ec and Ecl exhibited no obvious mediolateral gradient.

Immersion-fixed tissue. Calbindin immunoreactivity was overall lighter and less consistent in immersion-fixed tissue, but when observed at low magnification (4×), it appeared largely unaffected by fixation method (Fig. 7B). The granule cell layer of the dentate gyrus appeared darkly stained and contrasted nicely with the lower level of immunoreactivity in the adjacent molecular and polymorphic layers. However, significant differences were found when these preparations were observed at higher magnification (40× or higher). For example, the somas of the granule cells were clearly delineated in perfusion-fixed tissue (Fig. 7C), but often appeared so degraded in immersion-fixed tissue that it was impossible to identify individual neurons (Fig. 7D). This effect was present even at the shortest postmortem interval (2 hours) and did not seem to worsen in tissue subjected to longer postmortem intervals.

Calretinin

Perfused tissue. The distribution of calretinin-immunoreactive neurons and fibers reportedly exhibits important interspecies differences, even within families of Old World monkeys (Kobayashi and Amaral, 1999). We provide here a fundamental description of the distribution of calretinin-immunoreactivity in the rhesus monkey hippocampal formation (Fig. 8).

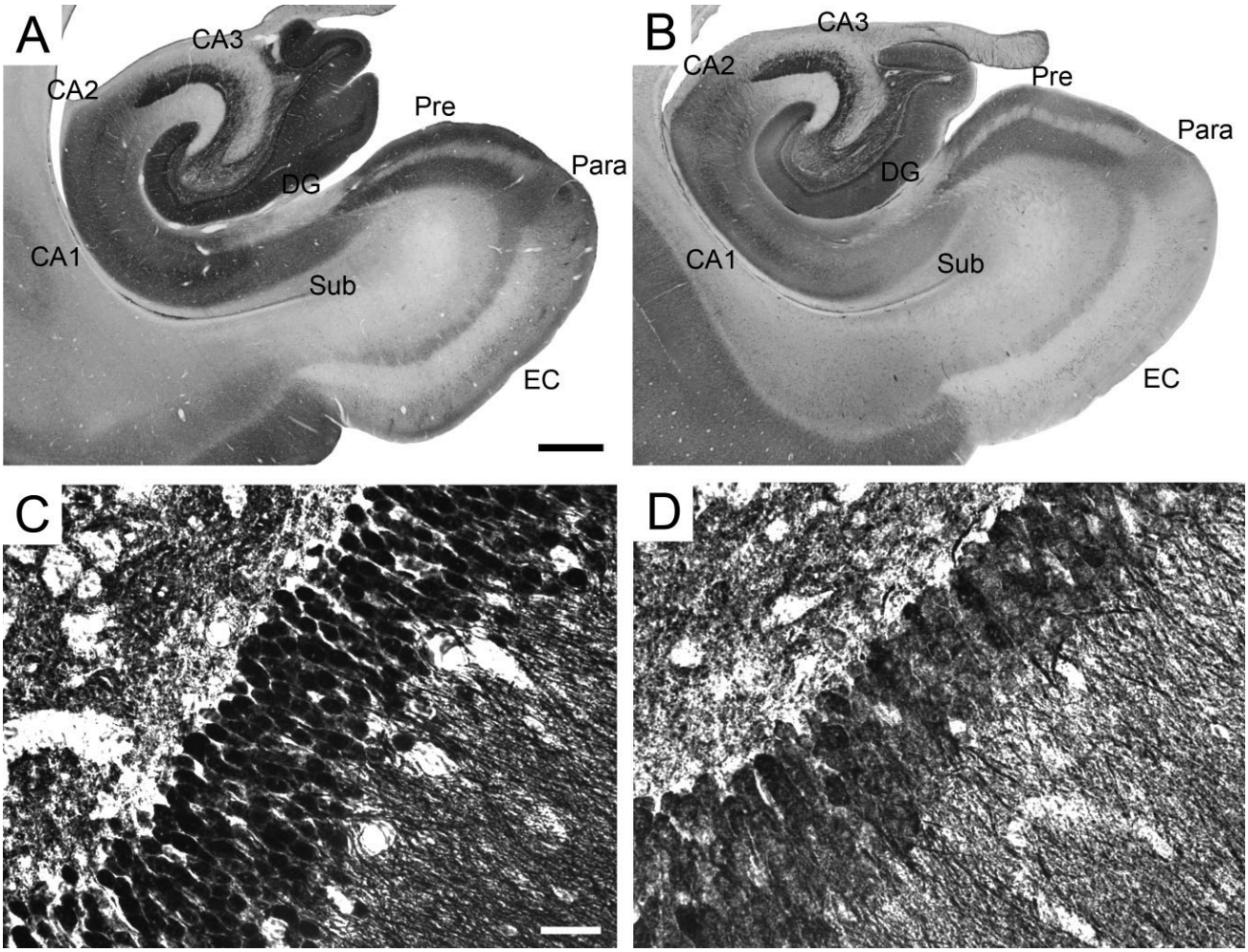

Figure 7.
Calbindin-D_{28k} immunoreactivity in the monkey hippocampal formation. **A,B:** Low-magnification photomicrographs of the distribution of calbindin-immunoreactive fibers and cells. A: PM-17-03, perfusion-fixed. B: PM-03-02, immersion-fixed 2 hours postmortem. **C,D:** High-magnification photomicrographs of the calbindin-positive dentate granule cells. C: PM-17-03, perfusion-fixed. D: PM-03-02, immersion-fixed 2 hours postmortem. Note the degradation of cellular labeling in immersion-fixed tissue. For abbreviations, see Fig. 1. Scale bars = 1 mm in A (applies to B); 30 μm in C (applies to D).

In the dentate gyrus, calretinin-positive cells were located primarily in the polymorphic layer and to a lesser extent in the granule cell and molecular layers. One cell type found in the polymorphic layer was a fusiform cell that had dendrites oriented largely parallel to the granule cell layer. Another cell type tended to be round and small, with dendrites perpendicular to and entering the granule cell layer. At least some of these cells were observed in the subjacent or within the granule cell layer itself, and were likely immature granule cells. The mossy fibers were inconsistently stained for calretinin. At rostral levels of the dentate gyrus, in particular at the level of the pes hippocampus, the polymorphic layer exhibited a dense diffuse labeling and we observed large, calretinin-positive multipolar cells (Fig. 8C). This dense diffuse labeling, however, showed significant interindividual variations in intensity. Interestingly, the number of large calretinin-immunoreactive multipolar cells, as well as their staining intensity, decreased rapidly at more caudal levels, and these cells were not detected in the caudal two-thirds of the dentate gyrus. There was an intense diffuse labeling in the inner one-third of the molecular layer and a distinctly denser band of diffuse staining just above and partly within the superficial margin of the granule cell layer. The diffuse staining in the inner one-third of the molecular layer also exhibited a rostral-to-caudal gradient in intensity, but remained visible throughout the entire extent of the dentate gyrus. Surprisingly, the distinct band of diffuse staining just above and partly within the superficial margin of the granule cell layer did not exhibit such a gradient. Similarly, neither the fusiform nor the small, round calretinin-immunoreactive neurons located in the polymorphic layer exhibited obvious rostrocaudal gradients. Occasionally, calretinin-immunoreactive cells were observed in the molecular layer.

In CA3 the highest density of calretinin-positive neurons was found in stratum radiatum, but labeled neurons were also found in the proximal portion of the pyramidal cell layer, and in

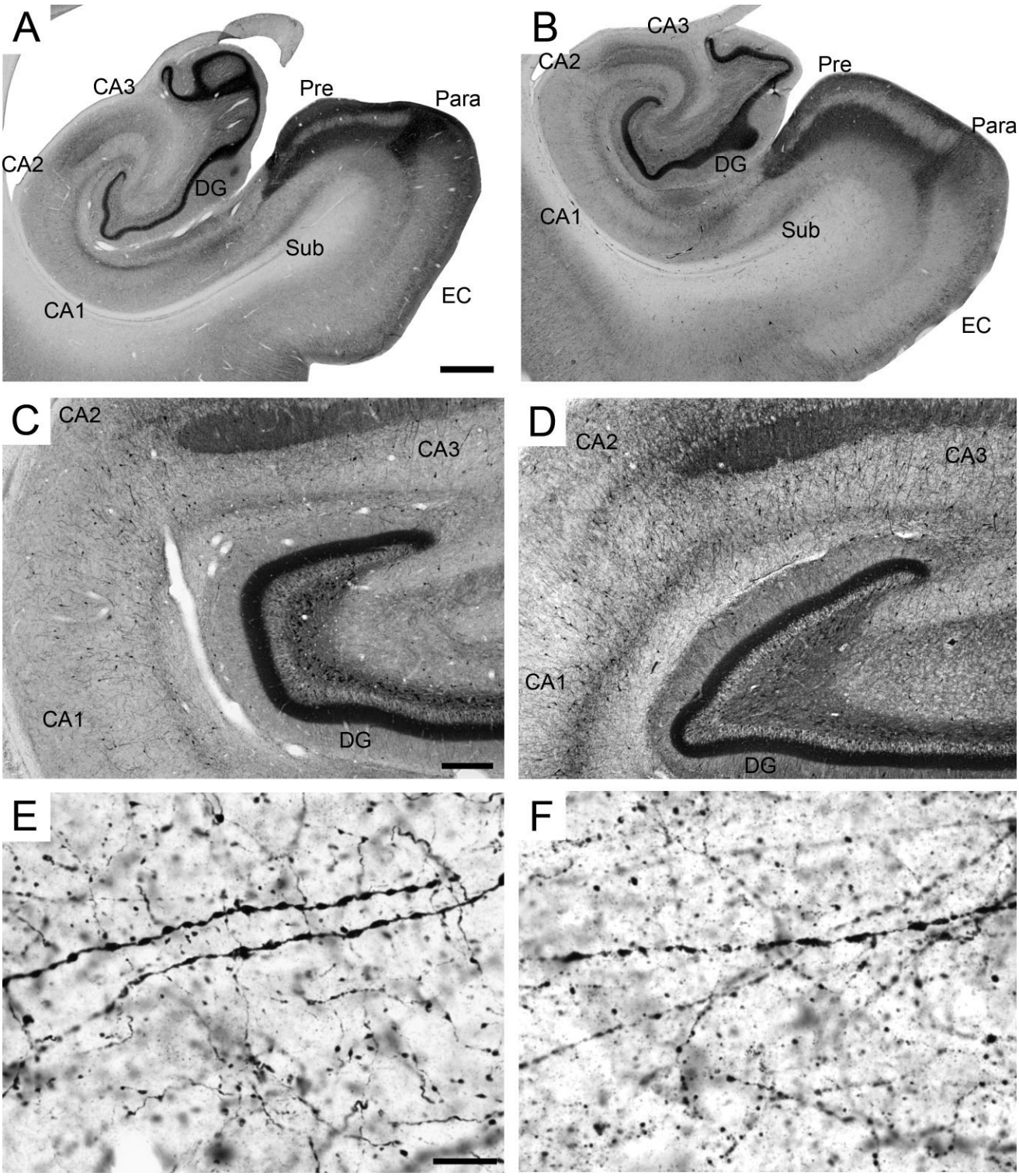

Figure 8.
Calretinin immunoreactivity in the monkey hippocampal formation. **A,B:** Low-magnification photomicrographs of the distribution of calretinin-immunoreactive fibers and cells. A: PM-17-03, perfusion-fixed. B: PM-02-02, immersion-fixed 2 hours postmortem. **C,D:** Intermediate magnification photomicrographs of calretinin-immunoreactivity in the rostral dentate gyrus, CA3, CA2, and CA1 fields of the hippocampus. C: PM-15-03, perfusion-fixed. D: PM-14-03, immersion-fixed 12 hours postmortem. Note the calretinin-positive neurons in the polymorphic layer of the dentate gyrus. **E,F:** High-magnification of calretinin-positive fibers in the stratum radiatum of the CA1 field of the hippocampus. E: PM-17-03, perfusion-fixed. F: PM-02-02, immersion-fixed 48 hours postmortem. Note the degradation of cellular labeling in immersion-fixed tissue. For abbreviations, see Fig. 1. Scale bars = 1 mm in A (applies to B); 300 μm in C (applies to D); 15 μm in E (applies to F).

strata lucidum and lacunosum moleculare. In CA2 and CA1 the highest number of immunoreactive neurons were present in the superficial portion of stratum radiatum. Fewer neurons were found scattered throughout stratum lacunosum-moleculare and the pyramidal cell layer. Only occasional calretinin-positive neurons were found in stratum oriens of CA3, CA2, and CA1. Calretinin-positive fibers and terminals were lightly and diffusely distributed throughout all layers of the hippocampus. The fiber density was substantially higher in CA2 and likely corresponded to the projection originating in the supramammillary nucleus of the hypothalamus (Gulyas et al., 1992, in the rat). The distribution of calretinin-immunoreactive fibers largely followed that of immunoreactive cell bodies, with the highest density in the superficial portion of stratum radiatum in CA1. Long and thick-beaded (Fig. 8E), calretinin-positive dendrites traversed the entire thickness of strata pyramidale and radiatum. Their density was highest proximally (closer to CA2) and few were observed distally, at the border with the subiculum.

In the subiculum the highest density of calretinin-positive neurons was found in the superficial portion of the pyramidal cell layer, particularly at the border with CA1. The density of calretinin-immunoreactive fibers was lower in the pyramidal cell layer of the subiculum than in strata oriens, pyramidale, and radiatum of CA1. Fiber density was similar in the molecular layer of the subiculum and the stratum lacunosum-moleculare of CA1.

Layers I and II of the presubiculum showed intense diffuse staining. Interestingly, the superficial portion of layer I showed a rostrocaudal gradient and was more lightly stained caudally. The superficial portion of layer II was largely unstained, conveying a tri-laminar appearance, but nevertheless contained a very high number of small round calretinin-immunoreactive cell bodies. A few stained cell somas were also found throughout the deeper portion of layer II, and in layer I at rostral levels. Throughout the neuropil of the parasubiculum there was an intense diffuse staining. Although fibers were not clearly visible, numerous calretinin-positive pyramidal cell somas were distributed throughout layer II of the parasubiculum.

Staining patterns varied greatly in the different subdivisions of the entorhinal cortex. In the olfactory division (Eo), fibers were distributed homogeneously throughout the layers and small, round, calretinin-immunoreactive cells were concentrated mainly in layer II. There was a high density of round calretinin-immunoreactive cells and fibers in layers II and III of areas Elr and Elc. There was also a very high density of calretinin-immunoreactive pyramidal cells in layer V of areas Er and Ei, which were surrounded by a dense diffuse staining of the neuropil and numerous fibers extending in layer III. Cells in layer VI were completely unstained, except for an occasional small neuron. Finally, in areas Ec and Ecl the highest density of small calretinin-immunoreactive cells was present in layer II, together with a few positive neurons scattered throughout layer III. The highest density of calretinin-immunoreactive fibers was found in layers I and II of areas Ec and Ecl, and a low density of calretinin-immunoreactive small round cells and fibers were found throughout the deep layers V and VI.

Immersion-fixed tissue. The overall pattern of calretinin immunoreactivity appeared largely unaffected by immersion fixation or postmortem interval (Fig. 8B), although the diffuse neuropil staining was generally lighter and less consistent than in perfusion-fixed tissue. However, significant differences were found when these preparations were observed at higher magnification (40× or higher). The varicose dendrites of the heavily stained neurons in the stratum pyramidale of CA1 were not as clearly defined in immersion-fixed tissue (Fig. 8E, F), and the degree of degradation correlated with postmortem interval. Specifically, dendrite staining was coarser, appearing as a series of discontinuous clumps rather than a series of beads linked by a continuous fiber. This phenomenon was also observed in the molecular layer of the dentate gyrus and throughout the other hippocampal regions.

The somas of the large multipolar cells located in the rostral polymorphic layer of the dentate gyrus were much less intensely stained in immersion-fixed tissue (Fig. 8C,D), but as there was a high degree of interindividual variability it was not possible to determine whether there was a correlation between postmortem interval and staining intensity. This was similarly the case for the calretinin-immunoreactive pyramidal neurons in layer V of areas Er and Ei. In contrast, the immunostaining of the small, round cell somas observed throughout the hippocampal formation did not appear to be affected by immersion-fixation or postmortem interval (Fig. 8C,D).

Somatostatin

Perfused tissue. The pattern of somatostatin immunoreactivity in the rhesus macaque hippocampal formation (Fig. 9) largely resembled that previously described in the cynomolgus monkey by Bakst et al. (1985). The antiserum used in this study, S320 raised against somatostatin $28_{1\text{-}12}$, stains significantly fewer neurons than other antisera such as S309, which recognizes somatostatin-28 (Bakst et al., 1985). In contrast, the clarity of stained fibers is reportedly greater with the S320 antibody used in this study.

Few S320-immunoreactive neuronal bodies were observed within the hippocampal formation, with the exception of a sizable population of S320-immunoreactive neurons of various morphologies in the polymorphic layer of the dentate gyrus (Fig. 9C). In contrast, extensive S320-immunoreactive fiber systems varied in density among different hippocampal regions. In the dentate gyrus, stained fibers were highly prominent in the outer two-thirds of the molecular layer, but relatively few in the inner one-third of the molecular layer and in the granule cell layer. The polymorphic layer also contained many S320-immunoreactive fibers and varicosities, the density of which was higher at rostral levels.

S320-immunoreactivity was found in all subdivisions of the hippocampus and was denser at rostral levels than at caudal levels. Stratum lacunosum-moleculare had the highest density of labeled fibers, and the plexus of immunoreactive fibers was denser in CA1 than CA3. Although stratum radiatum and the pyramidal cell layer contained relatively few immunolabeled fibers, there were numerous S320-immunoreactive fibers in stratum oriens. Stratum lucidum was mostly free of immunostained fibers, and the few fibers observed in this region were often oriented perpendicularly.

The pyramidal cell layer of the subiculum had a relatively lower density of S320-immunoreactive fibers, which contrasted with the heavily labeled CA1-subiculum border. The molecular layer and layer III of the subiculum were also labeled with a fairly high density of fibers.

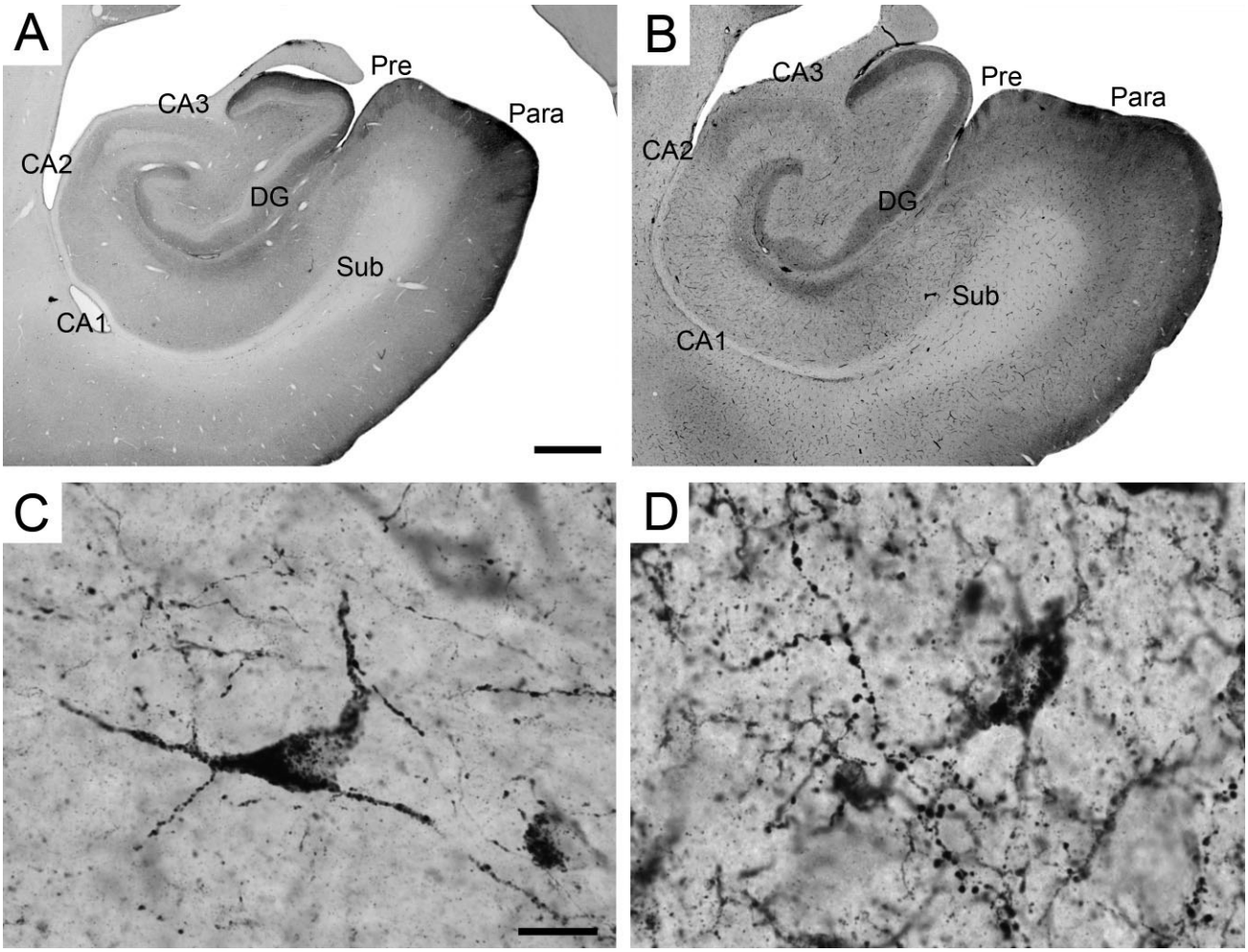

Figure 9.
Somatostatin (S320) immunoreactivity in the monkey hippocampal formation. **A,B:** Low-magnification photomicrographs of the distribution of S320-immunoreactive fibers. A: PM-15-03, perfusion-fixed. B: PM-05-02, immersion-fixed 6 hours postmortem. **C,D:** High-magnification photomicrographs of S320 immunoreactivity in the polymorphic layer of the dentate gyrus. C: PM-15-03, perfusion-fixed. D: PM-05-02, immersion-fixed 6 hours postmortem. Note the presence of large axonal varicosities and immunoreactive microglia in immersion-fixed tissue. For abbreviations, see Fig. 1. Scale bars = 1 mm in A (applies to B); 15 μm in C (applies to D).

In the presubiculum, a distinct laminar pattern of S320-immunoreactive fibers was evident. Throughout the rostrocaudal extent of the presubiculum, layer I contained a dense plexus of immunoreactive fibers. In layer II the superficial portion had a high density and the deeper part had a sparser distribution of labeled fibers. In the parasubiculum the molecular layer and layer II showed high densities of S320-immunoreactive fibers.

In the entorhinal cortex the distribution of S320-immunoreactivity varied rostrocaudally and mediolaterally. The density of S320-immunoreactive fibers was generally higher in the medial half than in the lateral half. At caudal levels where the cytoarchitecture of the entorhinal cortex becomes increasingly laminar, the stratification of fibers demonstrating S320-immunoreactivity also exhibited a more laminar pattern. The plexus of immunostained fibers was densest in layers I, III, and V.

Immersion-fixed tissue. S320-immunostaining was affected by immersion-fixation, even at the 2-hour postmortem interval (Fig. 9B). The densest zones of S320-immunoreactivity previously described in perfusion-fixed tissue could still be distinguished above background staining levels. However, the clarity of immunostained fibers was severely compromised, and in some cases they were nearly indistinguishable when observed under darkfield illumination at low magnification. Interestingly, large numbers of S320-immunoreactive microglia appeared throughout all fields of the immersion-fixed monkey hippocampal formation (Fig. 9D). Such labeling was never observed in perfusion-fixed tissue (Fig. 9C). However, control immunostaining procedures performed without the primary antibody raised against 5-HT revealed that the microglia staining was in fact due to nonspecific staining by the secondary antibody, goat antirabbit IgG (see also results for serotonin).

In addition, some features previously reported in human tissue could be distinguished in immersion-fixed tissue observed at high magnification (100×). Immunoreactive, grapelike clusters of apparently large, axonal varicosities were commonly observed in immersion-fixed monkey tissue (Fig. 9D), as has been previously observed only in human tissue (Amaral et al., 1988). These grapelike clusters of large varicosities were observed in tissue immersion-fixed even after 24 or 48 hours postmortem, even though fiber clarity decreased with increased postmortem interval in other hippocampal regions, such as the outer molecular layer of the dentate gyrus.

DISCUSSION

We have found several major and unexpected differences in the neuroanatomical characteristics of the hippocampal formation between perfusion-fixed and immersion-fixed monkey tissue. In some cases our results demonstrate that previously reported species differences are in fact due to methodological differences. In other cases comparison between immersion-fixed monkey tissue and human postmortem tissue suggests actual species differences. This study thus demonstrates unequivocally that in order to yield valid findings and conclusions regarding interspecies differences, morphological and neurochemical comparisons should be carried out with material prepared with identical methodology by the same personnel of one laboratory. Below, we summarize previous descriptions of the distribution of these markers in the human brain and discuss how our findings contribute to distinguishing between actual species differences and differences due to methodological factors.

Nissl stain

The differences in cell size between perfusion-fixed and immersion-fixed tissue were counterintuitive. Although overall brain volume was greater in immersion-fixed tissue, neuronal soma size was consistently smaller. Surprisingly, the degree of shrinkage varied considerably in different cell types, so that it was not possible to predict the soma size of a given neuronal population in immersion-fixed tissue based on perfusion-fixed values; instead, actual measurements of any particular cell type must be performed. Before evaluating how differential shrinkage might impact allometric comparison of cell size in different species, we discuss how our findings relate to previous estimates of cell size in rhesus monkeys obtained with different methodologies.

We first compared our findings regarding the volume of granule cells with those obtained in adult monkeys from three separate studies by Rosene and colleagues using intracellular biocytin filling techniques (St John et al., 1997; Luebke and Rosene, 2003; Ngwenya et al., 2006). We calculated an average volume of dentate granule cells, based on their published data of soma area, using the following formula: soma volume = 4/3 * surface area * (sqrt[surface area/3.1416]). This is the formula used by the nucleator probe (StereoInvestigator 5.0; MicroBrightField) to determine the volume of a cell (which corresponds to the formula used to determine the volume of a sphere of known radius; Cruz-Orive and Weibel, 1990). In a first study (St John et al., 1997), the average soma size was 65.7 μm^2, corresponding to a volume of 400 μm^3. The second study (Luebke and Rosene, 2003) reported an average soma size of 141 μm^2 (range 58–264 μm^2), corresponding to a volume of 1,259 μm^3. Finally, a third study (Ngwenya et al., 2006) reported an average soma size of about 100 μm^2 for mature granule cells, corresponding to a volume of 752 μm^3. In the current experiment, perfusion-fixation yielded an average granule cell soma size of 663 μm^3 (median 617 μm^3), whereas immersion-fixation yielded an average granule cell soma size of 245 μm^3 (median 228 μm^3). Such large differences in the estimated volumes of the granule cells may, among other factors, be due to methodological differences or interlaboratory differences (Scorcioni et al., 2004).

We also compared our findings regarding the volume of monkey CA1 pyramidal neurons in Nissl-stained preparations with those obtained in our laboratory from intracellular biocytin filling experiments (Altemus et al., 2005). It is important to note that the same fixative, 4% PFA, was used for both the Nissl-stained and biocytin-labeled preparations. The average volume of biocytin-labeled CA1 pyramidal neuron soma was 3,578 μm^3 (median: 3,472 μm^3). In comparison, the average soma size of CA1 pyramidal neurons determined in the Nissl-stained sections of this study was 4,282 μm^3 for perfusion-fixed tissue (median: 4,099 μm^3) and 3,154 μm^3 for immersion-fixed tissue (median 2,888 μm^3). In contrast to what was observed for the granule cells, volume estimates of monkey CA1 pyramidal cells obtained with different staining techniques, performed in our own laboratory, exhibited few differences. However, these data confirm that estimates of cell soma size are consistently lower in immersion-fixed tissue, as compared to those estimates obtained from perfusion-fixed tissue or intracellularly labeled cells.

How do these data in monkeys compare to estimates of cell soma size obtained in humans? Sà et al. (2000) reported estimates for soma volume of CA1 pyramidal neurons and nuclear volume of granule cells (which can be used as an approximation of soma cell volume due the scarcity of cytoplasm in granule cells). Human cerebral hemispheres were immersion-fixed in 4% PFA for at least 3 months. The average volume of CA1 pyramidal neurons was about 5,700 μm^3 and that of granule cells was about 480 μm^3. For CA1 pyramidal neurons (from brains immersion-fixed in 4% formalin no later than 24 hours postmortem), Jonsson et al. (1999) reported an average soma area of 353.4 μm^2, corresponding to a volume of about 4,998 μm^3. Arnold et al. (1995) reported an average soma size of 198.9 μm^2 for CA1 pyramidal neurons of neurologically normal subjects (volume: 2,110 μm^3), which is 58% to 63% smaller than the estimates by Sà et al. (2000), and Jonsson et al. (1999), respectively. However, in Arnold et al.'s (1995) study, blocks containing the hippocampus were immersion-fixed in alcohol fixative (70% ethanol, 150 nM sodium chloride) and embedded in paraffin prior to cutting and processing. Ethanol fixation-paraffin embedding procedures are known to produce greater shrinkage than PFA fixation-frozen sectioning procedures. The comparison of our data obtained in immersion-fixed monkey brains with those obtained in immersion-fixed human brains suggest that human hippocampal neurons might be about twice as big as monkey hippocampal neurons; granule cells: 480 μm^3 versus 245 μm^3 (1.96×); CA1 pyramidal neurons: 5,350 μm^3 versus 3,154 μm^3 (1.7×). However, as discussed above, these comparisons should be considered cautiously because of the considerable interlaboratory differences that can sometimes outweigh dif-

ferences between cell types or experimental conditions within a laboratory (Scorcioni et al., 2004).

In sum, neuronal soma volume was consistently smaller in immersion-fixed tissue compared to perfusion-fixed tissue. However, because we have found that different cell types from different brain regions react differently to immersion-fixation, it is not possible to determine a global correction factor to accurately predict the size of a given cell type following fixation by immersion or perfusion. Moreover, our findings raise questions regarding some methodology used to infer the differences in the size of specific cell types between different species. For example, Nimchinsky et al. (1999) inferred the existence of unusual, differentially enlarged projection neurons in the anterior cingulate cortex of humans and apes (whose brains had been immersion-fixed), based on the fact that other cell types in the cingulate cortex do not exhibit significant size differences between humans, apes, and other primate species (e.g., monkeys, whose brains had been perfusion-fixed). However, our data indicate that different cell types react differently to immersion-fixation. It is therefore difficult to draw clear conclusions about species differences when the samples from some species are immersion-fixed and the samples from other species are perfusion-fixed (Nimchinsky et al., 1999). Consequently, in order to be reliable, comparisons of even simple morphological features such as cell size should be carried out with material prepared using identical methodology and by the same personnel of one laboratory.

Nonphosphorylated high-molecular-weight neurofilaments

Our observation of substantial expression of nonphosphorylated NF-H in the CA2 field of perfusion-fixed monkey brain tissue contrasts with studies reporting only a low density of labeling in the human CA2 (Morrison et al., 1987; Vickers et al., 1994). Nevertheless, in our study the intensity of SMI-32 labeling was greatly decreased in the CA3 and CA2 of immersion-fixed tissue, which could explain the finding that CA2 has a relatively low level of SMI-32 immunoreactivity in human tissue.

Consistent with our findings, Vickers et al. (1994) identified very few cells and fibers that were SMI-32-immunoreactive in CA1. Interestingly, however, Vickers et al. showed this labeling pattern to be age-dependent. Whereas, young individuals (16-, 24-, and 43-year-olds) had few cells and fibers labeled, older control cases (47- and 66-year-olds) exhibited increased somato-dendritic labeling in individual CA1 neurons and patches of pyramidal cells. In another study, Morrison et al. (1987) reported that SMI-32 immunoreactivity is largely confined to the pyramidal cell layer and the polymorphic layer, with the lowest, but nevertheless detectable, density in CA2. They also showed that the subiculum has an extremely high density of SMI-32-immunoreactive cells and dendrites, whereas the pre- and parasubiculum have relatively low densities. Our observations of SMI-32-immunoreactivity in immersion-fixed monkey tissue are consistent with these patterns of labeling, except that we also find strong SMI-32 immunoreactivity in the mossy fiber pathway that was not present in the human tissue studied by Morrison et al. (1987).

Insausti and Amaral (2004) provided a very brief comparison of SMI-32 immunoreactivity in the monkey and human hippocampal formation. In monkeys, they reported that neurons in the CA3 and CA2 fields are heavily labeled, whereas neurons in CA1 are completely unstained. Neurons in the subiculum are also heavily stained, so much so that SMI-32 immunoreactivity provides a very useful marker for the borders of CA1 in monkeys. In contrast, CA1 cells in their human case (n = 1, 63 years old) were SMI-32-positive, consistent with the age-dependent reactivity observed in older control cases (47 and 66 years old) by Vickers et al. (1994). We did not observe any remarkable SMI-32-immunoreactivity in CA1 in our immersion-fixed monkey tissue. This suggests that the presence of heavy SMI-32 immunoreactivity in human CA1 is not due to a methodological difference (i.e., perfusion-fixation vs. immersion-fixation), but is rather linked to age-related changes in neuroskeleton organization. It remains to be determined, however, whether this pattern of CA1 staining observed in older human cases is also present in the brains of older monkeys (the monkeys used in the present study ranged from 4 to 17 years of age).

Insausti and Amaral (2004) indicated that in humans only some CA3 pyramidal cells were labeled, whereas the mossy fibers were heavily stained. Our findings in immersion-fixed monkeys revealed that in some cases SMI-32-immunoreactivity was reduced in CA3 and CA2 pyramidal neurons, whereas fusiform neurons in CA3 stratum oriens were intensely labeled. In contrast, the mossy fibers were consistently stained in immersion-fixed monkey tissue, but only occasionally in perfusion-fixed tissue. A study by Siegel et al. (1993) suggests that the increased mossy fiber staining might be due to the dephosphorylation of high-molecular-weight neurofilaments. Although SMI-32 immunoreactivity is primarily somatodendritic, SMI-31 (a related monoclonal antibody to a phosphorylated epitope of neurofilament) primarily labels axons of the mossy fiber projection and perforant path. Indeed, perfusion-fixed monkey sections treated with alkaline phosphatase to remove phosphate groups exhibit increased SMI-32 immunoreactivity throughout the hippocampus, including increased labeling of structures that normally label with antibodies to phosphorylated neurofilament proteins (Siegel et al., 1993). Our findings therefore suggest that the differential SMI-32 immunoreactivity pattern previously reported in human and monkey mossy fiber pathways (Insausti and Amaral, 2004) are in fact due to methodological differences (immersion-fixation in humans vs. perfusion-fixation in monkeys).

Acetylcholinesterase

The pattern of AChE staining observed in the hippocampal formation of perfusion-fixed or immersion-fixed monkey brains was very similar to that described for human postmortem preparations visualized enzymatically (Green and Mesulam, 1988) or immunohistochemically (De Lacalle et al., 1994). The only reported species difference in AChE staining is the thickness of the intensely stained band located in the molecular layer of the dentate gyrus, adjacent to the granule cell layer. In monkeys, there is a dense band of heavy AChE staining corresponding to the inner third of the molecular layer (Green and Mesulam, 1988; this study). In contrast in humans, the band of heavy AChE staining along the inner edge of the molecular layer is considerably thinner (Green and Mesulam, 1988; De Lacalle et al., 1994). At this time it is unclear whether the distribution of this diffuse labeling in the human molecular layer reflects 1) a differential organization of the local circuitry,

2) a scarcer cholinergic septal projection, or 3) a heavier projection from the entorhinal cortex, which in nonhuman primates has been shown to reach the outer two-thirds of the molecular layer (Witter et al., 1989). There are no other significant differences between AChE fiber distribution between monkeys and humans, indicating that the cholinergic innervation of the hippocampal formation is largely similar among primates and that monkeys constitute very good models to study the role of the cholinergic system in human cognitive functions.

Serotonin

Serotonin immunoreactivity was eliminated in immersion-fixed tissue, even at the shortest postmortem interval. This is consistent with the absence of serotonin immunoreactivity in postmortem human brains (Jones et al., 1992). Consequently, the study of the serotonergic system in immersion-fixed monkey or human brains is essentially based on the distribution of either serotonin receptors or transporters (see Kobayashi and Amaral, 1999, and references therein). 5-HT1 and 5-HT2 receptors have been localized to the dentate gyrus of monkeys and humans, but the precise laminar or cellular distribution is unknown. Similarly, both 5-HT1 and 5-HT2 receptors are distributed throughout the human and marmoset hippocampus. The density of 5-HT1a receptors is greater in CA1 than CA3, whereas the density of 5-HT1c receptors is equivalent in these two areas. 5-HT1b receptors have not been detected in the human hippocampus. Clearly, a comprehensive study detailing the distribution of serotonergic fibers, receptors, and transporters in the monkey hippocampal formation is essential, especially considering the prominent role that serotonin plays in several neuropsychiatric disorders.

Parvalbumin

The pattern of parvalbumin-immunoreactivity that we report here is nearly identical to that reported in the human dentate gyrus by Brady and Mufson (1997). The majority of parvalbumin-positive neurons occupied a zone of the polymorphic layer immediately subjacent to the granule cell layer, and only an occasional bipolar parvalbumin-stained neuron was observed in the granule cell and molecular layers. Our findings are also in agreement with the detailed description of Seress et al. (1993a) in humans, except for their report of the presence of a large number of immunoreactive neurons in the molecular layer of the dentate gyrus. Our experiments in monkeys did not indicate that immersion-fixation necessarily increased the number of parvalbumin-immunoreactive neurons in these areas. However, in the absence of systematic quantification such apparent discrepancies might derive from the subjective evaluation of staining patterns by different investigators. Thus, at this point, we do not believe that this difference should be considered as a proven species difference.

In the human hippocampus, Brady and Mufson (1997) reported a pattern that we have corroborated in the current study with immersion-fixed monkey tissue. The majority of parvalbumin-stained neurons occupy strata pyramidale and oriens, with an occasional immunoreactive neuron in stratum lacunosum-moleculare, and virtually no parvalbumin-positive neurons in stratum radiatum. In contrast, Seress et al. (1993a) suggested that although parvalbumin-containing neurons formed similar subpopulations in monkeys and humans, the human hippocampus nonetheless displays a larger variability in the morphology and location of parvalbumin-immunoreactive neurons.

The distribution of parvalbumin immunoreactive cells and fibers described in great detail in the human entorhinal cortex by Mikkonen et al. (1997) corresponds to that previously described in the monkey entorhinal cortex (Pitkänen and Amaral, 1993a,b) and by this study. In humans, the highest concentrations of parvalbumin-immunoreactive neurons are found in layers II and III. Only caudally, where the overall density of parvalbumin immunoreactivity is substantially greater, are a large number of immunopositive neurons and terminals found in the deep layers.

In sum, the overall staining patterns of parvalbumin-immunoreactive neurons and fibers are similar in the monkey and human hippocampal formation. Systematic comparison of monkey and human preparations using quantitative methods on tissue prepared by identical methodologies in the same laboratory are required to determine whether subtle interspecies differences previously reported in the literature represent actual differences or whether they derive from the subjective nature of the evaluations performed in the different studies.

Calbindin-D_{28K}

Sloviter et al. (1991) claimed that unlike the rat and the baboon, the human CA1 pyramidal neurons were not calbindin-positive and suggested that this may explain the greater vulnerability of CA1 pyramidal cells to ischemia. Seress et al. (1993a), in contrast, suggested that the distribution of calbindin-immunoreactive cells and fibers in the human hippocampal formation is fundamentally similar to that of the nonhuman primate (Seress et al., 1991). They reported that calbindin immunoreactivity is present in virtually all granule cells of the dentate gyrus and in a proportion of pyramidal neurons in CA2 and CA1. Moreover, they identified a distinct population of calbindin-positive neurons that is distributed in all layers of the dentate gyrus and hippocampus, but most frequently located in the molecular layer of the dentate gyrus and the pyramidal cell layer of the hippocampus. Finally, they also found that in the subiculum, immunoreactive nonpyramidal neurons are equally distributed in all layers, whereas in the presubiculum they occur mainly in the superficial layers. Findings from the current study largely corroborated these observed patterns, and thus confirmed the general conclusions of Seress et al. (1993a, 1991).

The discrepant results between Sloviter et al. (1991), and Seress et al. (1993a, 1991) and the current study cannot be explained by fixation methods (perfusion vs. immersion). Indeed, staining of CA1 pyramidal neurons appeared largely normal in immersion-fixed monkey tissue, even at high magnification (40×) and for postmortem intervals up to 48 hours. In contrast, however, the fixative solution used by Sloviter et al. (1991) was made of 2% PFA / 2% acrolein in 0.1 M PB (pH 7.4), whereas the solution used by Seress et al. (1993a) was made of 4% PFA, 0.1% glutaraldehyde, and 0.2% picric acid in 0.1 M PB (pH 7.4), and the current study used 4% PFA in 0.1 M PB (pH 7.4). In the absence of any other information, it is reasonable to hypothesize that the differences in immunostaining patterns resulted from the use of different fixative solutions.

In the human entorhinal cortex, calbindin-immunoreactive neurons, fibers, and neuropil were distributed throughout the

rostrocaudal extent (Mikkonen et al., 1997), in a pattern nearly identical to that found in the present study, with the rostromedial portions more intensely stained than caudolateral areas, and most of the calbindin-positive neurons located in the superficial layers rather than in the deep layers.

Thus, in sum, the distributions of calbindin D_{28K}-immunoreactive cells and fibers in the monkey and human hippocampal formation are remarkably similar. This similarity includes the presence of calbindin-positive pyramidal neurons in the CA1 region of the hippocampus.

Calretinin

The distribution of neurons and fiber systems that stain for the calcium-binding protein calretinin reportedly exhibits important interspecies differences, even within families of Old World monkeys (Kobayashi and Amaral, 1999). Importantly, in this study we found that the patterns of calcium-binding protein-immunoreactivity can vary significantly along the transverse and rostrocaudal axes of the rhesus monkey hippocampal formation (see also Seress et al., 2008).

Nitsch and Ohm (1995) reported that in humans, calretinin-immunoreactivity was present exclusively in nongranule cells of the dentate gyrus and in nonpyramidal cells of the hippocampus. Calretinin-positive neurons were found most frequently in the polymorphic layer of the dentate gyrus and in strata radiatum and lacunosum-moleculare of CA1, whereas neurons in CA2 and CA3 were rarely immunostained. The majority of these calretinin-immunoreactive neurons were small, bipolar, or fusiform neurons, and their dendritic trees were, for the most part, parallel to the dendrites of the principal cells.

In the polymorphic layer, they observed cells with dendrites parallel to the granule cell layer but restricted to the polymorphic layer. In general, dendrites were smooth or sparsely spiny, displaying small conventional spines. The axons which usually emerged from the proximal dendrite and could be followed over long distances, were thin, had small varicosities, and displayed only few collaterals that branched relatively far away from the cell body. Distinct bands of darkly stained calretinin-positive fibers occupied the innermost portion of the molecular layer and the pyramidal cell layer of CA2. They were, however, unable to detect a calretinin-positive cell type that has been described as specifically associated with the mossy fiber system in the rat hippocampus (Gulyas et al., 1992), and which is thought to correspond to the long-spined multipolar neuron also described in the rat by Amaral (1978). Therefore, Nitsch and Ohm concluded that the distribution of calretinin-immunoreactive structures in the human hippocampus is similar to that observed in African grey monkeys (Seress et al., 1993b), but differs from that described in rats (Gulyas et al., 1992).

However, Nitsch and Ohm (1995) specifically mention that their study was performed on material obtained from the midportion of the human hippocampus, at the level of the medial and lateral geniculate nuclei. This is the same level from which African grey monkey hippocampal tissue was obtained in the study by Seress et al. (1993b). Nitsch and Ohm (1995) thus noted that they could not rule out the possibility that the calretinin-containing spiny neurons (previously identified in the rat) are present in the human hippocampus at more posterior (caudal) and/or anterior (rostral) levels. Indeed, we have demonstrated the presence of such calretinin-positive neurons in the rostral portion of the polymorphic layer of the monkey dentate gyrus. Interestingly, Gulyas et al. (1992) suggested that in the rat these cells contribute to the commissural projections, which are prominent throughout the entire septotemporal (long) axis of the dentate gyrus. In contrast, the commissural projections of the monkey hippocampal formation originate only from the rostral (or uncal) portion of the dentate gyrus (Amaral et al., 1984), which corresponds largely to the region of the dentate gyrus in which we observed a large number of these calretinin-immunoreactive neurons in the polymorphic layer.

More recently, Seress et al. (2008) reported the presence of calretinin-positive mossy cells in the rostral portion of the polymorphic layer of the perfusion-fixed monkey brain (including rhesus monkey, African grey monkey, pig-tailed monkeys, and common marmosets), but not in immersion-fixed human brain. Our experimental data suggest, however, that the cellular staining of the large multipolar cells present in the rostral portion of the monkey polymorphic layer is very much reduced if not absent in immersion-fixed tissue. It is therefore possible that the species differences suggested by the Seress et al. study reflect methodological differences rather than true species differences between human and nonhuman primates.

Somatostatin

Studies of perfusion-fixed rat and monkey tissue have shown that, whereas antiserum S309 (directed against the first 14 amino acids of SS28) reveals a large population of stained neuronal cell somas, antiserum S320 (directed against $SS28_{1-12}$) preferentially highlights fiber systems in the hippocampal formation. In the human dentate gyrus, differential staining with these antisera was not as pronounced as in rats and monkeys (Amaral et al., 1988). In particular, antiserum S320 appeared to mark an equal number of neurons as compared to preparations incubated with antiserum S309, and the neurons tended to be labeled more extensively with S320 (e.g., with label extending into dendritic processes). These apparent species differences in immunoreactivity may be explained by Morrison et al. (1983), who suggest that SS28, primarily located in the neuronal cell body, is cleaved to form $SS28_{1-12}$, which is then rapidly transported away from the cell body. Following this logic, then, it is possible that during immersion fixation SS28 could be partially degraded to yield $SS28_{1-12}$, which would, in the absence of active transport, accumulate in the soma of neurons, thus leading to increased immunostaining.

Two other major species differences have been reported previously: 1) a higher density of somatostatin-positive fibers in the inner molecular layer in humans, as compared to monkeys, and 2) clusters of large, grapelike varicosities distributed throughout the dentate gyrus, especially in the polymorphic layer. We did not observe an increased density of somatostatin-positive fibers in the inner molecular layer of the dentate gyrus in immersion-fixed tissue. This suggests that the differential innervation of the molecular layer between monkeys and humans may represent a true species differences. In contrast, we did observe clusters of large, apparently axonal varicosities in the polymorphic layer of the dentate gyrus in immersion-fixed monkey tissue. These results indicate that this previously reported difference between monkeys and humans is in fact due to the method of fixation (i.e., perfusion vs. immersion).

CONCLUSION

Comparative studies of the structural organization of the brain from different species are fundamental to our understanding of human brain function. However, findings from the current study demonstrate unequivocally that what could be considered minute or insignificant differences in experimental procedures, such as the fixation of brains by perfusion of a fixative solution through the vasculature of a deeply anesthetized subject versus by immersion of postmortem tissue in the same fixative solution, can lead to fundamental changes in the morphological and neurochemical characteristics of particular cell types in different brain structures. Although this study focused on different regions of the hippocampal formation, we believe that the results have far-ranging implications for all experimental studies that use postmortem tissue to study any part of the brain. We have clearly shown that, besides less consistent staining patterns in immersion-fixed tissue, the manner in which differential fixation will impact the morphological and neurochemical characteristics of any particular cell type in any given structure of the brain cannot be predicted. Consequently, in order to yield valid findings and conclusions regarding interspecies differences, comparative neuroanatomical studies should be carried out with material prepared with identical methodology by the same personnel of one laboratory.

LITERATURE CITED

Altemus KL, Lavenex P, Ishizuka N, Amaral DG. 2005. Morphological characteristics and electrophysiological properties of CA1 pyramidal neurons in macaque monkeys. Neuroscience 136:741–756.

Amaral DG. 1978. A Golgi study of cell types in the hilar region of the hippocampus in the rat. J Comp Neurol 182:851–914.

Amaral DG, Campbell MJ. 1986. Transmitter systems in the primate dentate gyrus. Hum Neurobiol 5:169–180.

Amaral DG, Lavenex P. 2007. Hippocampal neuroanatomy. In: Andersen P, Morris RGM, Amaral DG, Bliss TV, O'Keefe J, editors. The hippocampus book. Oxford: Oxford University Press. p 37–114.

Amaral DG, Insausti R, Cowan WM. 1984. The commissural connections of the monkey hippocampal formation. J Comp Neurol 224:307–336.

Amaral DG, Insausti R, Cowan WM. 1987. The entorhinal cortex of the monkey: I. Cytoarchitectonic organization. J Comp Neurol 264:326–355.

Amaral DG, Insausti R, Campbell MJ. 1988. Distribution of somatostatin immunoreactivity in the human dentate gyrus. J Neurosci 8:3306–3316.

Arnold SE, Franz BR, Gur RC, Gur RE, Shapiro RM, Moberg PJ, Trojanowski JQ. 1995. Smaller neuron size in schizophrenia in hippocampal subfields that mediate cortical-hippocampal interactions. Am J Psychiatry 152:738–748.

Bakst I, Amaral DG. 1984. The distribution of acetylcholinesterase in the hippocampal formation of the monkey. J Comp Neurol 225:344–371.

Bakst I, Morrison JH, Amaral DG. 1985. The distribution of somatostatin-like immunoreactivity in the monkey *Macaca fascicularis* hippocampal formation. J Comp Neurol 236:423–442.

Banta Lavenex P, Amaral DG, Lavenex P. 2006. Hippocampal lesion prevents spatial relational learning in adult macaque monkeys. J Neurosci 26:4546–4558.

Benoit R, Bohlen P, Ling N, Briskin A, Esch F, Brazeau P, Ying SY, Guillemin R. 1982a. Presence of somatostatin-28-(1-12) in hypothalamus and pancreas. Proc Natl Acad Sci U S A 79:917–921.

Benoit R, Ling N, Bakhit C, Morrison JH, Alford B, Guillemin R. 1982b. Somatostatin-28(1-12)-like immunoreactivity in the rat. Endocrinology 111:2149–2151.

Brady DR, Mufson EJ. 1997. Parvalbumin-immunoreactive neurons in the hippocampal formation of Alzheimer's diseased brain. Neuroscience 80:1113–1125.

Cruz-Orive LM, Weibel ER. 1990. Recent stereological methods for cell biology: a brief survey. Am J Physiol 258(4 Pt 1):L148–156.

de Haas Ratzliff A, Soltesz I. 2000. Differential expression of cytoskeletal proteins in the dendrites of parvalbumin-positive interneurons versus granule cells in the adult rat dentate gyrus. Hippocampus 10:162–168.

De Lacalle S, Lim C, Sobreviela T, Mufson EJ, Hersh LB, Saper CB. 1994. Cholinergic innervation in the human hippocampal formation including the entorhinal cortex. J Comp Neurol 345:321–344.

Goldstein ME, Sternberger LA, Sternberger NH. 1987. Varying degrees of phosphorylation determine microheterogeneity of the heavy neurofilament polypeptide (NF-H). J Neuroimmunol 14:135–148.

Green RC, Mesulam MM. 1988. Acetylcholinesterase fiber staining in the human hippocampus and parahippocampal gyrus. J Comp Neurol 273:488–499.

Gulyas AI, Miettinen R, Jacobowitz DM, Freund TF. 1992. Calretinin is present in non-pyramidal cells of the rat hippocampus. I. A new type of neuron specifically associated with the mossy fibre system. Neuroscience 48:1–27.

Hof PR, Morrison JH. 1995. Neurofilament protein defines regional patterns of cortical organization in the macaque monkey visual system — a quantitative immunohistochemical analysis. J Comp Neurol 352:161–186.

Holmseth S, Lehre KP, Danbolt NC. 2006. Specificity controls for immunocytochemistry. Anat Embryol 211:1–10.

Hornung JP, Riederer BM. 1999. Medium-sized neurofilament protein related to maturation of a subset of cortical neurons. J Comp Neurol 414:348–360.

Insausti R, Amaral DG. 2004. Hippocampal formation. In: Paxinos G, Mai JK, editors. The human nervous system. Amsterdam: Elsevier. p 871–914.

Jones EG, Hendry SHC, Liu XB, Hodgins S, Potkin SG, Tourtellotte WW. 1992. A method for fixation of previously fresh-frozen human adult and fetal brains that preserves histological quality and immunoreactivity. J Neurosci Methods 44:133–144.

Jonsson SA, Luts A, Guldberg-Kjaer N, Ohman R. 1999. Pyramidal neuron size in the hippocampus of schizophrenics correlates with total cell count and degree of cell disarray. Eur Arch Psychiatry Clin Neurosci 249:169–173.

Kobayashi Y, Amaral DG. 1999. Chemical neuroanatomy of the hippocampal formation and the perirhinal and parahippocampal cortices. Handbook Chem Neuroanat 15:285–337.

Kobayashi Y, Amaral DG. 2000. Macaque monkey retrosplenial cortex: I. Three-dimensional and cytoarchitectonic organization. J Comp Neurol 426:339–365.

Lavenex P. 2008. Neuroanatomy methods in humans and animals. In: Squire LR, editor. New encyclopedia of neuroscience. Amsterdam: Elsevier.

Lavenex P, Amaral DG. 2000. Hippocampal-neocortical interaction: a hierarchy of associativity. Hippocampus 10:420–430.

Lavenex P, Suzuki WA, Amaral DG. 2002. Perirhinal and parahippocampal cortices of the macaque monkey: projections to the Neocortex. J Comp Neurol 447:394–420.

Lavenex P, Banta Lavenex P, Amaral DG. 2004a. Nonphosphorylated high-molecular-weight neurofilament expression suggests early maturation of the monkey subiculum. Hippocampus 14:797–801.

Lavenex P, Suzuki WA, Amaral DG. 2004b. Perirhinal and parahippocampal cortices of the macaque monkey: intrinsic projections and interconnections. J Comp Neurol 472:371–394.

Luebke JI, Rosene DL. 2003. Aging alters dendritic morphology, input resistance, and inhibitory signaling in dentate granule cells of the rhesus monkey. J Comp Neurol 460:573–584.

Mikkonen M, Soininen H, Pitkänen A. 1997. Distribution of parvalbumin-, calretinin-, and calbindin-D28k-immunoreactive neurons and fibers in the human entorhinal cortex. J Comp Neurol 388:64–88.

Morrison JH, Benoit R, Magistretti PJ, Bloom FE. 1983. Immunohistochemical distribution of pro-somatostatin-related peptides in cerebral cortex. Brain Res 262:344–351.

Morrison JH, Lewis DA, Campbell MJ, Huntley GW, Benson DL, Bouras C. 1987. A monoclonal antibody to non-phosphorylated neurofilament protein marks the vulnerable cortical neurons in Alzheimer's disease. Brain Res 416:331–336.

Ngwenya LB, Peters A, Rosene DL. 2006. Maturational sequence of newly generated neurons in the dentate gyrus of the young adult rhesus monkey. J Comp Neurol 498:204–216.

Nimchinsky EA, Gilissen E, Allman JM, Perl DP, Erwin JM, Hof PR. 1999. A neuronal morphologic type unique to humans and great apes. Proc Natl Acad Sci U S A 96:5268–5273.

Nitsch R, Ohm TG. 1995. Calretinin immunoreactive structures in the human hippocampal formation. J Comp Neurol 360:475–487.

Pitkänen A, Amaral DG. 1993a. Distribution of parvalbumin-immunoreactive cells and fibers in the monkey temporal lobe: the amygdaloid complex. J Comp Neurol 331:14–36.

Pitkänen A, Amaral DG. 1993b. Distribution of parvalbumin-immunoreactive cells and fibers in the monkey temporal lobe: the hippocampal formation. J Comp Neurol 331:37–74.

Rakonczay Z, Brimijoin S. 1988. Monoclonal antibodies to human brain acetylcholinesterase: properties and applications. Cell Mol Neurobiol 8:85–93.

Sà MJ, Madeira MD, Ruela C, Volk B, Mota-Miranda A, Lecour H, Goncalves V, Paula-Barbosa MM. 2000. AIDS does not alter the total number of neurons in the hippocampal formation but induces cell atrophy: a stereological study. Acta Neuropathol 99:643–653.

Saper CB, Sawchenko PE. 2003. Magic peptides, magic antibodies: guidelines for appropriate controls for immunohistochemistry. J Comp Neurol 465:161–163.

Scorcioni R, Lazarewicz MT, Ascoli GA. 2004. Quantitative morphometry of hippocampal pyramidal cells: differences between anatomical classes and reconstructing laboratories. J Comp Neurol 473:177–193.

Seress L, Gulyas AI, Freund TF. 1991. Parvalbumin- and calbindin D28k-immunoreactive neurons in the hippocampal formation of the macaque monkey. J Comp Neurol 313:162–177.

Seress L, Gulyas AI, Ferrer I, Tunon T, Soriano E, Freund TF. 1993a. Distribution, morphological features, and synaptic connections of parvalbumin- and calbindin D28k-immunoreactive neurons in the human hippocampal formation. J Comp Neurol 337:208–230.

Seress L, Nitsch R, Leranth C. 1993b. Calretinin immunoreactivity in the monkey hippocampal formation. I. Light and electron microscopic characteristics and co-localization with other calcium-binding proteins. Neuroscience 55:775–796.

Seress L, Abraham H, Czeh B, Fuchs E, Leranth C. 2008. Calretinin expression in hilar mossy cells of the hippocampal dentate gyrus of nonhuman primates and humans. Hippocampus 18:425–434.

Siegel SJ, Ginsberg SD, Hof PR, Foote SL, Young WG, Kraemer GW, McKinney WT, Morrison JH. 1993. Effects of social deprivation in prepubescent rhesus monkeys — immunohistochemical analysis of the neurofilament protein triplet in the hippocampal formation. Brain Res 619:299–305.

Sloviter RS, Sollas AL, Barbaro NM, Laxer KD. 1991. Calcium-binding protein (calbindin-D28K) and parvalbumin immunocytochemistry in the normal and epileptic human hippocampus. J Comp Neurol 308:381–396.

St John JL, Rosene DL, Luebke JI. 1997. Morphology and electrophysiology of dentate granule cells in the rhesus monkey: comparison with the rat. J Comp Neurol 387:136–147.

Sternberger LA, Sternberger NH. 1983. Monoclonal-antibodies distinguish phosphorylated and nonphosphorylated forms of neurofilaments in situ. Proc Natl Acad Sci U S A 80:6126–6130.

Suzuki WA, Porteros A. 2002. Distribution of calbindin D-28k in the entorhinal, perirhinal, and parahippocampal cortices of the macaque monkey. J Comp Neurol 451:392–412.

Vickers JC, Riederer BM, Marugg RA, Bueescherrer V, Buee L, Delacourte A, Morrison JH. 1994. Alterations in neurofilament protein immunoreactivity in human hippocampal neurons related to normal aging and Alzheimers disease. Neuroscience 62:1–13.

Witter MP, Van Hoesen GW, Amaral DG. 1989. Topographical organization of the entorhinal projection to the dentate gyrus of the monkey. J Neurosci 9:216–228.

Zimmermann L, Schwaller B. 2002. Monoclonal antibodies recognizing epitopes of calretinins: dependence on Ca^{2+}-binding status and differences in antigen accessibility in colon cancer cells. Cell Calcium 31:13–25.